NUMERICAL SIMULATION OF BLOCH EQUATION FOR PROTONS IN WATER AND FAT MOLECULES

By

Birtukan Asega Tadesse

A THESIS SUBMITTED TO

THE PROGRAM OF GRADUATE STUDIES OF
ADDIS ABABA UNIVERSITY

IN PARTIAL FULFILLMENT OF THE REQUIREMENTS
FOR THE DEGREE

MASTER OF SCIENCE in PHYSICS

ADDIS ABABA, ETHIOPIA

JULY 2018

ADDIS ABABA UNIVERSITY

PROGRAM OF GRADUATE STUDIES

NUMERICAL SIMULATION OF BLOCH EQUATION FOR PROTONS IN WATER AND FAT MOLECULES

By

Birtukan Asega Tadesse

Department of Physics

Addis Ababa University

Approved by the Examining Board:

Dr. Tesfaye Kidane Signature _____
Advisor

Dr. Deribe Hirpo Signature _____
Examiner

Dr. Chernet Amante Signature _____
Examiner

Dated: July 2018

ADDIS ABABA UNIVERSITY

Date: **July 2018**

Author: **Birtukan Asega Tadesse**

Title: **Numerical Simulation of Bloch equation for protons in Water and Fat Molecules**

Department: **Department of Physics**

Degree: **M.Sc.** Convocation: **June** Year: **2018**

Permission is herewith granted to Addis Ababa University to circulate and to have copied for non-commercial purposes, at its discretion, the above title upon the request of individuals or institutions.

_____

Signature of Author

This Work is Dedicated

to

My Mam and Dad

Table of Contents

List of Figures

Acknowledgements

One of the pleasures of writing this thesis is acknowledging the effort of many people whose names may not appear on the cover, but whose hard work, cooperation, friendship and understanding were crucial to the success of this thesis work. There fore, I would like to take the opportunity to express my sincere gratitude to all, whom I can name out and who have highly devoted their time, knowledge and resources to the completion of this thesis. The Almighty GOD, I would like to praise for His blessings and blissfulness, He gave me to pass all these moments and finalize the paper. My Advisor, Dr.Tesfaye Kidane, for the encouragements, guidance, critics and recommendations throughout my thesis. He is a great mentor and his encouragement on a daily basis, exceptional role he has played and he helped me as friendly approach. Without his offering to accomplish this research, I would not be able to finish my study. Addis Ababa University, physics department teachers and students, for their help, advices and recommendations in my two year studies. My sponsor, Dilla University, for giving me the opportunity to build up my capacity for my better contribution towards the development of the home land country. To my beloved and faithful family for always been there to support me no matter how far or occupied they are. They had all the love and faith in me to complete my two year course in physics. I would also like to thank all my friends for their encouragement and supportive ideas.

Addis Ababa University

Birtukan Asega Tadesse

July, 2018

Nomenclature

T_1	Longitudinal relaxation time
T_2	Transverse relaxation time
2D	Two dimensional
O	Oxygen
C	Carbon
H	Hydrogen
ΔE	Energy difference
h	Plank's constant
Δf	Frequency difference
^0K	Degree kelvin
B_1	Radiofrequency field
FID	Free Induction Decay
SNR	Signal to Noise Ratio

Abstract

The phenomenological time dependent Bloch equations have been a source of insight about the magnetic resonance phenomena and the purpose of this study was to solve the Bloch equations in the laboratory frame. First, the time- dependent Bloch equations were reduced to a homogeneous linear differential equation, and then a simple equation was derived to solve it using a matrix operation (diagonalization method). Then, as an example, this method is applied to the time dependent Bloch equations for protons in water and fat molecules in uniform static field. The radiofrequency (RF) pulse is first applied to disturb the protons so that they fall out of alignment with the static magnetic field. This disturbance occurs through the transfer of energy from the RF pulse to the protons, that can only occur when the RF pulse has the same frequency as the Larmor frequency of the protons. The representative trajectories of transverse component describe the complete time evolution of magnetization in the transverse component. The transverse magnetization behaviour can be described by transient sinusoidal oscillation. This has been observed due to the interaction with neighbouring spin, the amplitude magnetization damped and oscillates sinusoidal with time that can considerably vary for different matters, depending on the size of the time constant T_2 . For example, for water, T_2 are quite high, dephasing of the transverse magnetization are slow. For fat, however, relaxation process are considerably faster. Hence, this work clearly describes the effect of tissue properties (T_2 relaxation time) of the proton of both water and fat if they are exposed in a homogeneous field in the sample. The Fourier transformation of the time domain leads Lorentzian peak in the frequency spectrum in given sample.The matlab simulation results give the more physical insight about the behaviour of magnetization.

CHAPTER 1

Introduction

1.1 Background of the study

Magnetic Resonance Imaging (MRI) is a tomographic imaging technology that uses radio waves and a magnetic field to produce the image of internal, physical and chemical characteristics of an object from externally measured Nuclear Magnetic Resonance (NMR) signals [1]. NMR is technique of obtaining the signal from the entire sample and used to investigate the structure and dynamics of molecules by analysing the magnetic properties of the nuclei without encode the location of sample [2, 3]. In contrary MRI is the method of separating a sample and constructing images based on the entire signal from the nucleus in each voxel.MRI has become an indispensable tool in diagnostic radiology. It reveals fine details of anatomy,yet is non-invasive methods for looking inside the body without opening up the body surgically and does not require ionizing radiation such as X-rays. Furthermore, it is a highly flexible technique so that contrast between one tissue and another in an image can be varied simply by varying the way the image is made. The source of the flexibility of MRI lies in the fact that the measured signal depends on several properties of the tissue. This is distinctly different from other types of radiological imaging.

In computer tomography (CT), for example, the image is a map of one local property of the tissue: the X-ray absorption coefficient. Similarly, in nuclear medicine studies, the image is a map of the radioactive tracer concentration. But, in MRI, the image is a map of the local transverse magnetization of the hydrogen nuclei. This transverse magnetization, in turn, depends on several intrinsic properties of the tissue. In fact, the transverse magnetization is a transient phenomenon; it does not exist until we start the MRI process. The fact that the MR signal depends on a number of tissue properties is the source of its flexibility, but it is also a source of difficulty in developing a solid grasp of MRI. To understand the full range of MRI applications, it is necessary to understand the basic physics of NMR and how the

MR signal can be manipulated experimentally.

In the early 20^{th} century, it became clear that classical physics could not account for the world of atoms and subatomic particles. Experiments showed that the light emitted from excited atoms consisted of discrete frequencies, suggesting that only certain energy states could exist rather than a continuum of states. To explain subtle but distinct splitting of some of these spectral lines, called the hyperfine structure, Pauli proposed in 1924 that atomic nuclei possess an intrinsic angular momentum (spin) and an associated magnetic moment. The interaction of the electrons in the atom with the magnetic field of the nucleus creates a slight shift in the energy levels and a splitting of the spectral lines. The significance of these small effects is that they provide a window to investigate the basic properties of matter. From the magnitude of this hyperfine structure, one could estimate the magnitude of the nuclear magnetic moment, but the precision of these experiments was poor. In the 1930s, new techniques were developed based on the deflection of molecular beams in an inhomogeneous magnetic field [4], but these techniques were still inadequate for precision measurements.

During World II war, Purcell worked at the Massachusetts Institute of Technology on radar development [5] and Bloch worked at Harvard on radar countermeasures, and their experience with radio frequency (RF) techniques and measurements may have contributed to the success of their NMR studies [6]. Even though, the experiments performed by them were different, it was quickly realized that they were looking at two different aspects of the same phenomenon: in a magnetic field nuclei precess at a rate proportional to the field, with the spin axis rotating at a characteristic frequency. Purcell showed that electromagnetic energy is absorbed by a material at this resonant frequency, and Bloch showed that the precessing nuclei induce a detectable oscillating signal in a nearby detector coil. In both experiments, magnetic properties of the nucleus are manifested in terms of a frequency of electromagnetic oscillations, which can be measured with very high precision. In the next few years, NMR became a key tool for investigating atomic and nuclear properties based on these small effects of nuclear magnetization. Finally, in 1952, Purcell and Bloch were awarded the Nobel Prize in Physics for the development of NMR techniques and the contributions to basic physics made possible by NMR [7, 8].

For first time in 1950's the relationship between chemical shift and chemical structure in a high-resolution H^1 spectrum of ethanol were demonstrated by Arnold, Dharmatti

and Packard.

A key development in the methodology used in these chemistry applications was the introduced by Richard Ernst(1960's) of Fourier transform methods for acquiring and analyzing the signal. Rather than sweeping the magnetic field to excite each spectral line in turn, all of the nuclei are excited at once and the spectrum is sorted out from the combined signals using the Fourier transform. This same basic methodology has carried through to current MRI methods [7]. In the development of NMR, 1970's is outstanding year in the investigation of clinical images. In 1971, Raymond Damadian of the state university of New York discovered T_1 and T_2 , relaxation times were significantly longer in cancerous rat tissue than in the corresponding normal tissue [8]. After that in 1973, Paul Lauterbur observed the first 2D image of water sample and after four years Mansfield got first image of both human finger and abdomen [5, 9]. In MRI,resonance frequency of a nucleus depends on the static magnetic field, but it is also influenced by the local electronic environment (surrounding nuclei) because the electrons in the molecules shield the nucleus altering the local magnetic fields.This effect is called the chemical shielding which reflects the local electronic environment [10]. For example, the electronic shielding of the protons in the triglyceride molecules of fat is greater than that experienced by protons in water molecules, resulting in different microscopic magnetic fields, and subsequently different proton resonance frequencies [10, 11]. Fat has a complex spectrum with multiple peaks, the largest of which is shifted down field by ≈ 3.5 ppm from the water peak as shown in Fig.1.1. The water

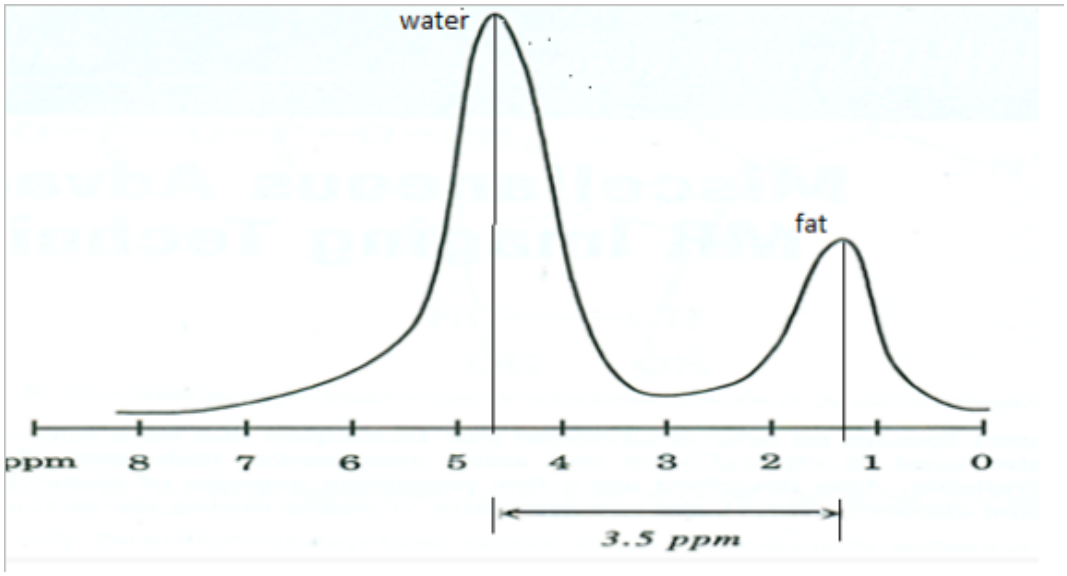

Figure 1.1: Schematic spectrum peaks for fat and water over a large anatomic area broadened due to surrounding nuclei.

molecule is a composed of two hydrogen atom and oxygen atom that the proton is attached to. Hence, oxygen (O-3.5) in the water has higher electronegativity than carbon (C- 2.5) in the fat molecule and then carbon in fat molecule is more shielded than oxygen in water molecule. In chemical environment, the higher electronegative of the atom that the proton is attached to, the proton is less shielded, and they required a greater magnetic field to produce that chemical shift. This indicates they have greater energy difference between the spin states ($\Delta E = h\Delta f$) and this energy difference correspond to the higher frequency absorption in the system. Therefore, signal formed by less shielded molecules forms higher frequency signal. Thus, the resonance frequency difference (also referred to as chemical shift) provide the information about the proton inside the molecules undergo resonance relative to reference resonance frequency such as tetramethylsilane(TMS) is a volatile inert compound that gives a single peak up field which have position of reference peak of 0ppm.

In NMR the reorient of the molecule in the applied magnetic field is related with the molecular size of the molecule. Molecules which have small molecular size and rapidly rotating molecules (e.g.free water), with a polar character due to its electronegative oxygen atom. Water molecule reorient more rapidly, relax more slowly because of the slow energy transfer process (long T_1 and T_2 times) and the resulting image is sharply contrasting image. On the other hand the bound molecules (like fat) exists in the tissues as a long chain triglycerides and they have larger molecular size compared with water, fat will rotate slower than water molecules. This implies the slower the tumble rate of the fat enables a faster relaxation rate [12, 13].

In addition in the case of fluid the term viscosity describes a measure of the capacity of the fluid being deformed by shear stress or the fluid internal resistance to flow (thickness of internal Fiction). In addition some experiment was done by comparing the thickness (or viscosity) of the honey and water and the result indicates that the less viscous the fluid is, the greater its movement (consistency or fluidity) of the molecule [14].

1.2 Motivation and objective

Todate, a simulation of the MR-effect in the context of MRI is especially relevant for clinical diagnostics, clinical studies, and the definition of measurement protocols. This is because simulation within the clinical environment can simplify the measur-

ement process. The sequence can be tuned algorithmically instead by experience removing the strain of finding suitable parameters. A simulation tool could also anticipate problems that are likely to occur and provide an option to control those problems directly incontrast to indirect tweaking of raw sequence parameters. The post-processing steps could be enhanced by adding knowledge, gained by a virtual simulation of a patient-specific experiment.

Image sets acquired with different sequences are commonly interpreted individually, because they are not directly comparable. For example, the acquired NMR signal of proton in the tissue depends on the surrounding molecules of the tissue. A simulation can connect the information and derive more robust and physiological parameters from the compound data. It is also feasible to conjoin images acquired with differing sequence, differin g hardware specifications. Numerical simulators of Bloch equations are essential tools for a variety of different research directions in MRI. For example, MRI pulse sequence optimization goes through several steps of parameter modifications until desired image characteristics are obtained. It is therefore a time consuming process and hence Bloch equation based numerical simulators are suitable, inexpensive tools for such purposes. Due to controlled experiments with the input data, numerical simulations can be used effectively to locate the exact sources of the artifacts, i.e. whether the artifacts are generated due to some physical phenomena (motion etc.) or hardware malfunctions. Apart from the controlled experiments with precise input data, numerical simulators can also be used to simulate various limiting experimental conditions which are either improbable or difficult to reproduce in experiments. Because of this advantage, it is a very useful pedagogical and educational tool.

The basic idea for numerical simulation of MRI images is to solve repeatedly the Bloch equation for each volume element (voxel) in the sample (in our case, water and fat). Actually for each voxel the Bloch equation has to be considered twice. The Bloch equation has to be solved a first time during the resonance process to get the position of the magnetisation vector (M) at the end of the resonance. It is during this stage that we have to take into account the effects of RF field perturbations. The position of M at the end of the resonance process is the initial position of M for the relaxation process. Then, the Bloch equation has to be solved a second time during the relaxation process. As the RF field is stopped during the relaxation, there is no RF field disturbances to be taken into account for this stage. In this thesis, we present a numerical solution of M to the time dependent Bloch

equation in a laboratory frame for protons in water and fat molecules. Here, the computational cost of the method reduces to the computation of the eigen-elements of a block tridiagonal matrix of a very small size (3x3).

1.3 Thesis structure

This thesis is organized into five chapters. In Chapter 1 (Introduction), we begin with background and motivation of the study and continues with other basic components of MRI scanner. In Chapter 2 (Principle of MRI), the basic physics underlying NMR is reviewed in details. In Chapter 3 (Methodology), we have presented a method to solve numerically the time dependent Bloch equation and we have justified it from a mathematical point of view. In Chapter 4 (Results and Discussion), the results and and discussion are presented. The final chapter (Chapter 5) summarises the results of the present study and draws general conclusions about this work. At last, we recommend about future work in this area of the study.

1.4 Hardware components of MRI scanner

MRI machine has similar frame work to the CT scan machine but they differ by their performance and modality employed in capturing the images. MRI machine (a tube like structure, which is called the bore) systems can be described in terms of five main components; magnet, RF coil, shim coil, gradient coil, and control (Computer) subsystems. These are the main and basic hardware components of MRI scanner (see Fig.1.2).

1.4.1 The main field

The main magnetic field describes the strength in uniform static permanent field and it is powerful (typically for 1.5 tesla (T) magnet is 3×10^4 times stronger than the Earth's magnetic field) [3]. It is one of the major component of MRI. In addition, it is the biggest and most expensive part of scanner, because it is not easy to build a system to generate a gigantic magnetic field that is also quite uniform. Typically, for clinical purpose, the range of the field strength is in between 0.1 to 3.0 T. The main magnetic field is produced by current flowing in the main coils. Apart from other components the main magnet is always switched on [15, 13]. The basic purpose of the main field is to align the hydrogen (proton) to allow for the mapping of the tissue properties. There are three kinds of main magnet in a given scanner. These are Superconducting, Resistive and Permanent magnets. However, the majority of modern scanners utilize superconducting magnets because they

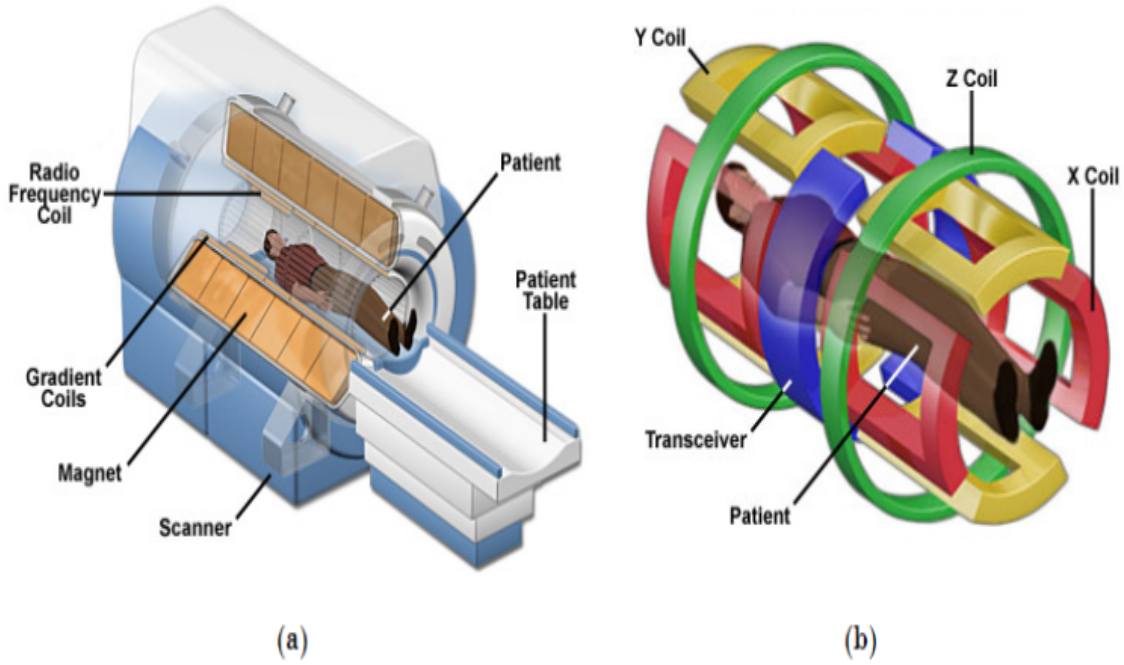

Figure 1.2: The hardware components of MRI Scanner: (a) Cutaway and (b) Gradient Magnets [16].

are capable to generate much larger fields, with high magnetic field homogeneity [3]. This magnet made up of materials such as copper coils which are embedded loops of NbTi (niobium-titanium or niobium-tin alloy), thus, as long as the coils are immersed by liquid helium to 4.2 ^{0}k, it becomes superconductor and this is capable of producing a very powerful magnetic field. The construction of such magnets is very expensive. Nowadays, this type of superconducting magnets is the most familiar MRI scanners [3].

1.4.2 RF coils

RF coil is the most important component of MRI machine which produce alternating current and this generates an electromagnetic field to disturb uniform alignment of the nuclear spin or magnetization. For this purpose the RF sends the electromagnetic waves (radio waves) that resonate at a particular frequency (determined by the strength of the magnetic field) in to the body [15, 17]. These coils provide two purposes:The transmit coil used for the disturbance of the coherence spins by sending electromagnetic energy to a sample at its resonant frequency.The process of rotation of the net magnetization away from thermal equilibrium orientation of parallel alignment is called excitation.In conventional MRI, this RF pulse is generated by means of a resonant cavity or near-field coil placed either around or next to the tissue. The other type is receive coil used to detect the raw MR signal by

receiving electromagnetic energy emitted by the sample at its resonant frequency and these process is called detection[18].
During the relaxation of the spins, receive coils (in some systems these are the same as transmit coils) collect the signal, which are computer analysed with numerical methods. The transmit RF coils produce the B_1 field used to tip or perturb the magnetization away from its equilibrium position. Once the magnetization is tipped to the desired angle, the transmit field is turned off and the receive coils are used to detect the signal.

The strength of magnetic field of the RF coils is proportional to the sensitivity of the coil. Apart from the main magnetic field the RF coils and gradient coil are switched on only when the image acquisition is performed [19, 20].

1.4.3 Gradient coils

The gradient coils are loop of wires that produce linearly varying time dependent magnetic fields that are added or subtracted from the static magnetic field which causes to vary the resonance frequency of the protons. These coils consist of three independently varying magnetic field within the sample which can be referred as x, y and z gradient coils [20, 21]. The basic purposes of these coils are to encode the position of the protons in which the signals were formed. The MRI imaging system uses the three independent gradient coils which is applied lying inside the bore of MRI scanner to perform the slice selection and encoding purposes. This important process is performed after the excitation process takes place and then gradient coils turned on to provide the spatial encoding needed to resolve an image. This component is the base for the image construction. Without gradient coil, imaging is impossible. In the imaging process, the gradient coil will be switched on and off many times. The typical value of gradient coils produce gradient strength in the order of tens mT/m [22].

1.4.4 Shim coils

In MR imaging, the inhomogeneity of the field must be removed before the imaging process takes place. The process of removing of inhomogeneities in the main magnetic field by putting the shimming coils is called shimming. There are two techniques of shimming; Fixed and Dynamic shimming.

Fixed shimming

Passive shimming involves the positioning of pieces of iron metal (steel) around the magnet, with the amount and position of the steel usually determined by a computer program. Active shimming involves the use of additional coils (the coil a little larger radius than the primary coil) in which currents of accurately determined magnitude are running [23]. The shim coils in superconducting magnets may also be positioned inside the cryostat, i.e. they are also superconducting. The required currents are determined during system installation and remain fixed until the service engineers re-shim the magnet.

Dynamic shimming

Dynamic shimming may be performed by the user to optimize the homogeneity over a given volume on a perpatient basis. Simple dynamic shimming involves the use of the gradient coils to produce the necessary static magnetic fields to optimize the uniformity. The required gradient magnetic fields are calculated either manually or automatically. In spectroscopy where < 0.1 ppm over a 10 mL volume is desirable, the manufacturer may offer an additional set of resistive (i.e. non-superconducting) shim coils, which may be manually or automatically adjusted. The usual optimizing techniques are to minimize the line-width of a Fourier-transformed free induction decay (FID) or to analyse phase-difference images.

1.4.5 Control

In MRI, the over all functions of the system is controlled by a computer workstation. The computer system is the most essential part which performs several activities: switched on and off the RF coils and gradient coils, accept the analogue data from RF coils and converting the data from analogue to digital [13].

To understand in simple word how the MR machine works, there are three types of magnets in MRI machine: primary place the patient into a main magnet that is capable of producing a strong, field to polarize the sample, latter sent RF wave in the body and the proton in the body absorb energy that comes from the varying magnetic field produced by RF coils which disturb the alignment of spins into the transverse plane by reducing the magnetization in the longitudinal direction. This process release in energy in the form of NMR signals which is measured by receive coil. Subsequently, the gradient coil is added to the system used to deliberately vary the main magnetic field and made to encode the position of information of the desired signal in the x, y and z axes that is called localization and all the signal

from the given sample is picked up by receive RF coil. Most of this works like receiving, recording, analysing images of the scanned body and interpreting the data were operated and controlled by the powerful computer system.

In MRI imaging process, there is local deformation of the image (called an artifact) that reduce the accuracy of an image [24, 25]. These results in the signal variation due to inhomogeneity in the static magnetic field and RF field inhomogeneity which is because of the nature of objects being imaged and also the manufacturing engineering trouble of magnetic coils. The field inhomogeneity affects the amplitude of the signal and the consequence of Bo field inhomogeneity is the blurring, distortion and signal loss at the tissue interfaces. The effect of RF field inhomogeneity sources a non-uniform effect on the spins [21].

CHAPTER 2

Principle of MRI

2.1 Introduction

In this chapter, the basic physics underlying NMR is reviewed and presented in more detail. We begin with a review of the basic physics of magnetic fields. The dynamics of a magnetic dipole in a magnetic field, which is the central physics underlying NMR, is considered next in terms of the two important physical processes of precession and relaxation.These two processes have quite different characteristics; precession is a rotation of the magnetization without changing its magnitude, whereas relaxation creates and destroys magnetization. The inter-play of these two processes leads to a rich variety of dynamic behaviour of the magnetization.

The physical picture presented here is a classical physics view, and yet the physics of a proton in a magnetic field is correctly described only by quantum mechanics. The source of the NMR phenomenon is that the proton possesses spin, and spin is intrinsically a quantum mechanical property. Despite the familiar name, spin is fundamentally different from the angular momentum of more familiar scale objects. For example, a spinning baseball possesses angular momentum, and yet we can easily imagine changing that angular momentum by spinning it faster or stopping it altogether. In other words, the spin is not an intrinsic part of the baseball. However, for a proton, the spin is an intrinsic part of being a proton. It never speeds up and never slows down, and the only aspect of the spin that can be changed is the orientation of the spin axis.

Fortunately, however, the classical view, although totally incorrect in its description of the behaviour of a single proton, nevertheless gives the correct physics for the average behaviour of many protons, and accurately describes most of the physics encountered in MRI [7]. For this reason, in this thesis, we will develop a physical picture of NMR based on a classical view, and the only feature from quantum mechanics that is essential is the existence of spin itself.

2.2 Induction and NMR signal detection

From the concept of electricity and magnetism , charges at rest create electric fields and charges in motion (currents) create magnetic fields. In the first half of the 20^{th} century, Faraday unravelled an additional feature: changing magnetic fields create electric fields. This phenomenon, called electromagnetic induction, is at the heart of many examples of electrical technology. For example, induction makes possible the generation of electricity from a mechanical energy source, such as hydroelectric power, and the conversion of acoustic signals into electrical signals in a microphone.

Fig.2.1 illustrates a spinning magnetic dipole inducing currents in several nearby coils. Generally, in MRI, coils are used for generating the main magnetic field for generating gradient fields used for imaging, for generating the oscillating radiofrequency (RF) field used to tip over the local magnetization, and for detecting the NMR signal. Induction is the process that generates a measurable signal in a detector coil.

Imagine a small dipole moment, a spinning charged sphere, rotating around an axis perpendicular to its spin axis. The spinning sphere creates a dipole magnetic field in its vicinity, and as the magnet rotates the dipole field sweeps around as well. As a result, at any fixed point in space near the magnetic dipole, the magnetic field changes cyclically with time. If we now place a loop of wire, a detector coil, near the spinning dipole, the changing magnetic field will produce a current in the wire through the process of induction (see Fig.2.1). The strength of the induced current in the coil depends on both the proximity and the orientation of the coil with respect to the magnetic dipole. The quantitative relation is that the induced current is proportional to the rate of change of the flux of the magnetic field through the coil. For example, consider a circular coil and imagine the surface enclosed by the wire. The net flux of the magnetic field is evaluated by adding up the perpendicular components of the magnetic field lines at each point on this surface. Or, more qualitatively, the flux is proportional to the number of field lines enclosed by the coil.

The concept of magnetic flux indicates that a flow of something through the coil, but the thing “flowing” is the magnetic field.Thus,the term magnetic fields and velocity fields in a fluid have closer analogy.

Velocity is also a vector, velocity field lines in an incompressible fluid also form closed loops, like magnetic field lines. Placing our coil in the fluid, the calculated flux is simply the volume flow rate through the coil. When the coil is perpendicular to the local flow direction, the flux is high; if the coil is placed so that the flow passes over it rather than through it, the flux is zero. When the coil is oriented such that the axis of the coil is the same as the axis of rotation of the dipole, the flux is constant so there is no induced current. On the other different orientations

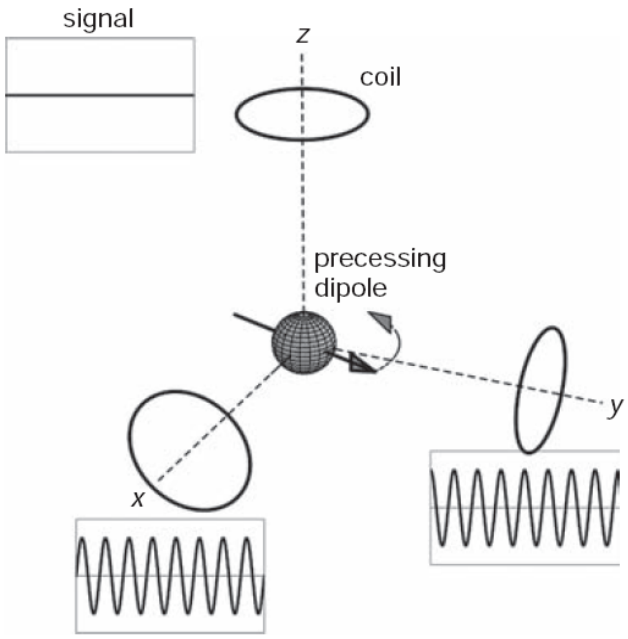

Figure 2.1: Induction signals in coils near a precessing magnetic dipole. For a dipole rotating in the x-y plane, coils along the x- and y-axis show oscillating signals with a relative phase shift of 90^o as the magnetic flux of the dipole passes across the coils. For the coil along the z-axis, the flux is constant, and so no current is induced.

though, a cyclic signal is generated in the coil with the same frequency as the frequency of rotation of the dipole. The maximum signal is produced when the axis of the coil is perpendicular to the axis of rotation of the dipole, because this orientation creates the largest change in flux as the dipole field sweeps(cross) past the coil. When the coil is moved farther from the source, the flux is diminished, and so the change in flux also is diminished, and the signal created in the coil is weaker.

The two coils oriented 90^o (which is equivalent to $\frac{\pi}{2}$ radians) from each other, but with the axis of each coil perpendicular to the rotation axis, show the same strength of induced current, but the signals are shifted in time. This time shift of the signal

is described as a phase shift, and in this case it is a phase shift of $\frac{\pi}{2}$. For any periodic signal with a period T, a shift in time can be described as an angular phase shift in analogy with circular motion. A phase shift of one full period T corresponds to one complete cycle, a phase shift of 2π, and a time shift of T/4 corresponds to a phase shift of $\frac{\pi}{2}$.

In MRI,the concept of phase dispersion and a resulting loss in signal is important in virtually all MRI techniques. Let us imagine a coil detecting the signal from several rotating dipoles. If the dipoles are all rotating in phase with one another, so that at any instant they are all pointing in the same direction, then the signals induced by each in the coil add coherently and create a strong net signal. However, if there is phase dispersion, so that at any instant the dipoles are not aligned, then there is destructive interference when the signals from each dipole are added together in the coil, and the net signal is reduced. Quadrature detector is an example of the configuration of two coils which are perpendicular to each other. Each coil is sensitive to the component of the magnetization perpendicular to the coil because that is the component that creates a changing flux through the coil. Because of their orientation, the signal measured in the second coil is phase-shifted $\frac{\pi}{2}$ from the signal in the first coil. By electronically delaying the second signal for one quarter of a cycle, the two signals are brought back in phase and can be averaged to improve the SNR before being sent to the amplifier. Because the two coils are oriented perpendicular to each other, the fluctuating fields that cause noise in one coil have no effect on the other coil. If the fluctuating fields along these two directions are statistically independent, the noise signals measured in the two coils will also be independent. Then, when the signals from the two coils are combined, the incoherent averaging of the noise improves the SNR by $\sqrt{2}$ compared with a single-coil measurement [7]. The other coil arrangement is phased array coil, two or more coils send signals to separate amplifiers, with the result that the detected signals are analysed individually [3]. Phased array coils are useful for imaging as a way of improving the SNR beyond what can be achieved by quadrature detection alone [26]. The noise picked up by a coil is proportional to its sensitive volume, which is linked to the size of the coil. Therefore, a small diameter coil obtains a better signal with a higher signal-to-noise ratio than a coil with a large diameter, but the drawback of a small diameter coil is that only a small region can be imaged. With a phased array system, several small diameter coils can be used to achieve the coverage of a large coil but with the SNR of a small coil. Each coil is sensitive to a different location and so provides a high SNR for the signal from that location.

Note that this requires separate amplifier channels for each coil. If the signals from the different coils were combined before being sent to a single amplifier, the noise from each coil would contaminate the signals from the other coils, destroying the SNR advantage.

2.3 Dynamics of nuclear magnetization

In the previous section, we see the magnetic field created by a magnetic dipole. We can now return to discuss the basic NMR experiment in terms of the basic physics (see Fig.2.2). The interaction of magnetic dipole moment of the atomic nucleus and

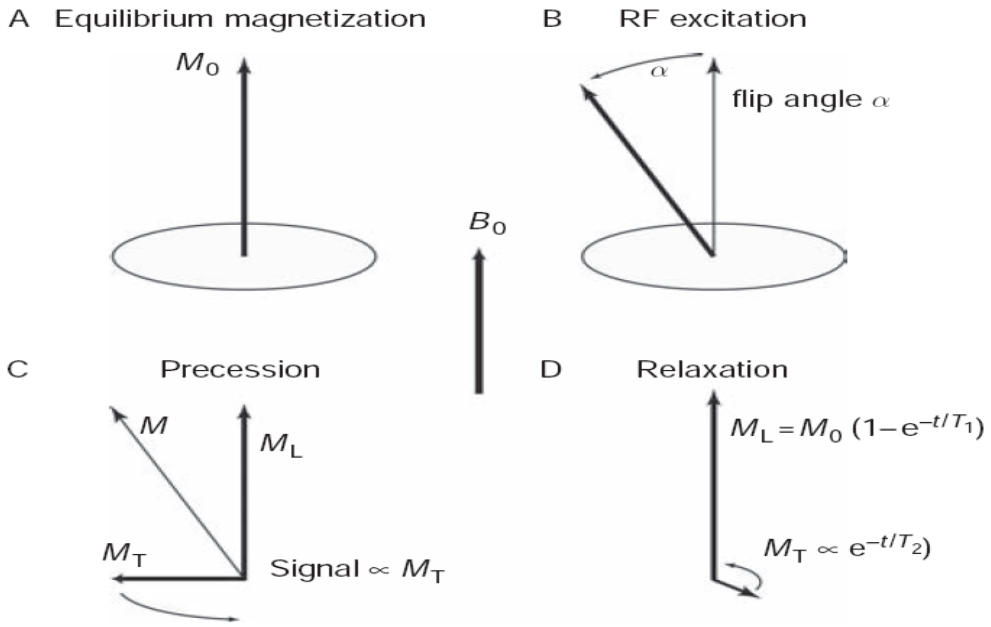

Figure 2.2: The basic physics of the NMR experiment: (A) In a magnetic field B_o, an equilibrium magnetization M_o forms from the alignment of nuclear dipoles (B.C). A radiofrequency (RF) pulse tips over M_o (B), creating a longitudinal component M_z and a transverse component M_{xy} (C). Then, M_{xy} precesses around the direction of B_o, generating a detectable NMR signal. (D) Over time, M_{xy} decays to zero with a relaxation time T_2 and M_z recovers to M_o with a relaxation time T_1. [27]

the local external magnetic field is characterized by two main effects. The first is that the field exerts a torque on the dipole that tends to twist it into alignment with the field, and the second is that in a non-uniform field there is a force on the dipole pulling it toward the region of stronger field. To understand these effect consider a magnetic dipole in a magnetic field.This dipole has the lowest energy when it is aligned with the field, and the energy progressively increases as the dipole is tipped away from the field. The highest energy configuration is when the dipole is

aligned opposite to the field. Similarly, the energy of the dipole is lower when it is in a stronger field, so it is aligned toward the larger field.

2.3.1 Equilibrium magnetization (M_o)

In a sample of water molecule, each H nucleus is a magnetic dipole; the oxygen nucleus (^{16}O) contains an even number of protons and neutrons and so has no net angular momentum nor a net magnetic moment. The spin axes of the individual H nuclei precess around the field, and over time they tend to align with the field. However, this alignment is far from complete. Exchanges of energy between the orientation of the dipole and thermal motions prevent the dipoles from settling into their lowest energy state. In fact, the energy difference between an H nucleus aligned with the field and one opposed to the field at 1.5 T is only approximately 1% of the random thermal energy of the water molecule. The result is that at equilibrium the difference between the number of spins aligned with the field and the number opposed to the field is only approximately 1 part in 10^5. Nevertheless, this creates a weak M_o aligned with the field. The term M_o (see Fig.2.2 A) is the net dipole moment per cubic centimetre, and one can think of it loosely as a weak, but macroscopic, local magnetic field that is the net result of summing up the magnetic fields of each of the H nuclei. That is, each cubic centimetre of a uniformly magnetized sample carries a net dipole moment M_o. The magnitude of M_o is directly proportional to the local proton density (or spin density). Mathematically, it is given by

$$M_o = \frac{\rho_o \gamma^2 \hbar^2}{4\kappa T} B_o, \tag{2.1}$$

where ρ_o is the proton density, γ is the gyro-magnetic ratio, $\hbar = \frac{h}{2\pi}$, κ is the Boltzmann constant, T is the tissue temperature, and B_o is the main magnetic field.

2.3.2 Precession

A magnetic dipole placed in a magnetic field experiences the same two important effects: a torque tending to align the dipole with the field and a force drawing it toward regions of stronger field.A spinning charged particle constitutes a magnetic dipole moment and the dipole moment (μ) is proportional to its angular momentum L. Faster rotation increases the angular momentum as well as the current produced by the charges on the surface, and so also increases the magnetic moment. Because of this intimate link between angular momentum (L) and the magnetic dipole moment (μ), the ratio of the two is a constant called the gyromagnetic ratio $\gamma = \frac{\mu}{L}$.

Each nucleus that exhibits NMR has a unique value of γ. The presence of angular momentum makes the dynamics of a magnetic dipole in a magnetic field distinctly different from the dynamics of an electric dipole in an electric field. As mentioned earlier, the effect of the field is to exert on the dipole a torque that would tend to twist it into alignment. Physically, torque is the rate of change of angular momentum given by

$$\tau = \frac{d\mathbf{L}}{dt} = \gamma \mathbf{L} \times \mathbf{B}_o. \tag{2.2}$$

Precession comes about because the torque axis is perpendicular to the existing angular momentum around the spin axis.The change in angular momentum produced by the torque is a change in the direction of spin, not the magnitude. Thus, the angular momentum (and the spin axis) precesses around the field.

This is an example of the nature of angular momentum and is exactly analogous to the behaviour of a spinning top or bicycle wheel. A spinning top tipped at an angle to the vertical would be in a lower energy state if it simply fell over; instead, the rotation axis precesses around a vertical line (see Fig.2.2 C). When put in the external magnetic field, the individually aligned parallel or anti- parallel protons spin in a particular way called precession. The frequency of precession is how many times the protons precess per second and is determined by the Larmor equation. (ω_o), is γB_o; the stronger the field, the stronger the torque on the dipole and the faster the precession. The precession frequency $\omega_o = \gamma B_o$ is the resonant frequency of NMR.

2.3.3 Relaxation

From the process of precession, one might conclude that a proton would never align with the main field, because the energy is lower. However, in a real sample, B_o is not the only source of magnetic field. The magnetic moments of other nuclei produce additional, fluctuating magnetic fields. For example, in a water molecule, an H nucleus feels the field produced by the other H nuclei in the molecule. Because the molecules are rapidly tumbling in their thermal motions, the total field felt by a particular nucleus fluctuates around the mean field B_o. These fluctuations alter both the magnitude of the total magnetic field and the direction felt by that nucleus. As a result, the proton's precession is more irregular, and the axis of precession fluctuates. Over time, the protons gradually tend to align more with B_o, through the process called relaxation [28]. Note that relaxation (see Fig.2.2 D) is a much slower process than precession: relaxation times on the order of 1s are approximately 10^8 times longer than the precession period with a typical MRI

magnet.

First, when a sample is exposed in a magnetic field, then the magnetic dipoles are randomly oriented so that the net magnetization is zero. This means that the dipoles possess a higher energy based on their orientation than they would if they were partly aligned with the field. The lowest possible energy would correspond to complete alignment. As the system relaxes, this excess energy is dissipated as heat; the dipoles align more with the field, and the longitudinal magnetization M grows toward its equilibrium value M_o.

For example in pure water sample, the main source of a fluctuating magnetic field that produces relaxation is the field produced by the other H nucleus in the same water molecule. But the presence of other molecules in the liquid (e.g., protein) can alter the relaxation rate by changing either the magnitude or the frequency of the fluctuating fields. A large molecule will tumble more slowly than a water molecule and, as a result, a water molecule that transiently binds to the large molecule will experience more slowly fluctuating fields. The magnitude of the fluctuating fields can be increased significantly in the presence of paramagnetic com- pounds. Paramagnetic compounds have unpaired electrons, and electrons have magnetic moments more than a thousand times larger than a proton. This is the basis for the use of paramagnetic contrast agents as a way of reducing the local relaxation time.

The relaxation time constant along the magnetic field, creating the net magnetization M_o, is T_1 and varies from approximately 0.2 to 4.0 s in the body [7]. The fact that T_1 varies by an order of magnitude between different tissues is important because this is the source of most of the contrast differences between tissues in MR images. The T_1 variations result from differences in the local environment (e.g., chemical composition or biological structures). In general, the higher the water content of a tissue, the longer the T_1. In MRI, the value of M_o depends on the density of dipoles and the magnetic field, but the value of T_1 required to reach this equilibrium depends on the environment of the spins.

The relaxation time constant T_1 is called the longitudinal relaxation time because it describes the relaxation of the component of the magnetization that lies along the direction of B_o. The other two relaxation times are T_2 and $T_2^\star$ describe the decay of the transverse component of the magnetization. At equilibrium, the magnetization is aligned with B_o, so there is no transverse component. Application of a 90^o radio frequency pulse tips the magnetization into the transverse plane, where it

precesses and generates a signal in a detector coil by induction. In a homogeneous field, the transverse component, and therefore also the NMR signal, decays away with a time constant T_2, and this process often is abbreviated as transverse relaxation. In the human body at field strengths typical of MR images, T_1 is approximately 8-10 times larger than T_2.

In the experimental work one finds that the NMR signal often decays more quickly than would be expected for the T_2 of the sample. This is qualitatively described by saying that the decay time is $T_2^\star$, with $T_2^\star$ less than T_2. The reason for this is simply inhomogeneity of the magnetic field. If two regions of the sample feel different magnetic fields, the precession rates will differ, the local transverse magnetization vectors will quickly get out of phase with each other, and the net magnetization will decrease through phase dispersion. However, this signal decay results from constant field offsets within the sample and not the fluctuating fields that produce T_2 decay. Because of this, the additional decay caused by inhomogeneity is reversible with a spin echo.

As mentioned in the next section, the combined processes of precession and relaxation are mathematically described by the Bloch equations, a set of differential equations for the three components of the magnetization. These are the basic dynamic equations of NMR and are used frequently to describe the behaviour of the magnetization.

2.3.4 The radiofrequency pulse excitation

The fact that the magnetic dipole moments of protons tend to align with the field, producing a net magnetization M_o, does not lead to any measurable signal (a constant magnetic field produces no currents). However, if M_o is tipped away from the direction of B_o, it will precess; all the nuclear dipoles will precess together if they are tipped over, so M_o also will precess at the same frequency.
The local value of M_o is the net difference between dipoles aligned with the field and opposite to the field, but it is not directly observable because it is many orders of magnitude weaker than B_o. However, if all the dipoles that contribute to M_o could be tipped $\pi/2$, they would all precess around the field at the same rate. Thus, M_o would also tip $\pi/2$ and begin to precess around the main field. Tipping over the magnetization produces a measurable, transient signal, and the tipping is accomplished by the RF pulse. During the transmit part of the basic NMR experiment, the oscillating RF current in the coil creates in the sample an oscillating magnetic field B_1 perpendicular to B_o.The magnitude of RF field is smaller than main field. Nevertheless, this causes the net magnetic field, the vector sum of B_1

and B_o, to wobble slightly around the B_o direction. Initially M_o is aligned with B_o, but when the net field is tipped slightly away from B_o, M_o begins to precess around the new net field. If the oscillation frequency of B_1 is different from the precession frequency ν_o, not much happens to M_o except a little wobbling around B_o. But if the RF frequency matches the precession frequency, a resonance phenomenon occurs. As the net magnetic field wobbles back and forth, the magnetization precesses around it in synchrony. The effect is that with each precessional rotation M_o tips farther away from B_o, tracing out a growing spiral as shown in Fig.2.3. After a time, the RF field is turned off, and M_o then continues to precess around B_o. The net effect of the RF pulse is thus to tip M_o away from B_o, and such pulses are usually described by the flip angle they produce (e.g., a $\pi/2$ pulse or a $\pi/6$ pulse). The flip angle can be increased either by increasing the amplitude of B_1 or by leaving B_1 on for a longer time.

angles. From an energetic point of view, tipping the net magnetization away from B_o increases the orientational energy of the dipoles: the nuclei absorb energy from the RF pulse. This transfer of energy is possible even with small B_o fields because B_o oscillates at the resonant frequency of the nuclei, the precession frequency. This is much like pushing a child on a swing. The swing has a natural resonant frequency, and giving very small pushes at that frequency produces a large amplitude of motion. That is, the swing efficiently absorbs the energy provided by the pusher when it is applied at the resonant frequency.

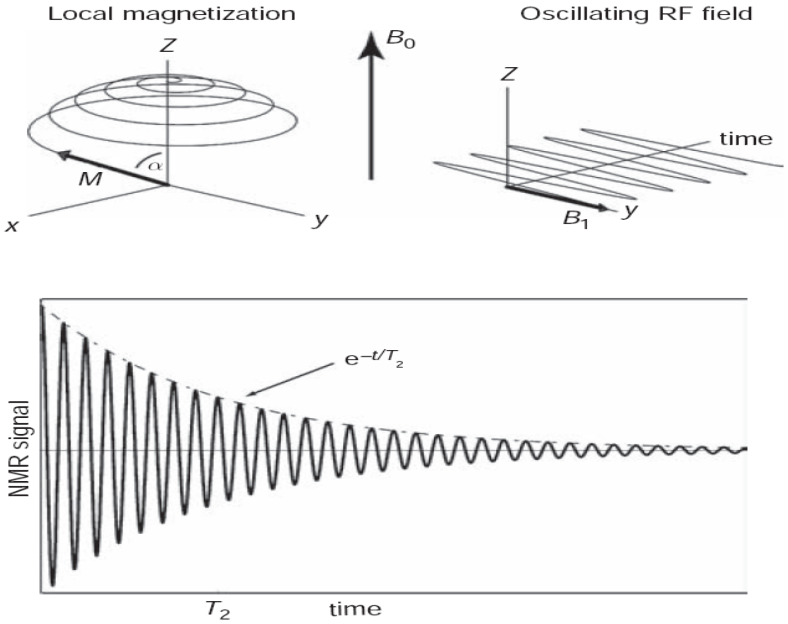

Figure 2.3: (Top plots)The arrangement of an equilibrium magnetization (M_o) as a result of partial alignment of nuclear magnetic dipoles. In the absence of a magnetic field, the spins are randomly oriented, and there is no net magnetization. When placed in a magnetic field B_o, the spins partly align with the field, a relaxation process with a time constant T_1 of approximately 1s, creating a net local magnetization. (Bottom plot) Free induction decay. After a $\pi/2$ radiofrequency pulse tips the longitudinal magnetization into the transverse plane, a detector coil measures an oscillating signal, which decays in amplitude with a time constant T_2 in a perfectly homogeneous magnetic field. The plot is not to scale; typically the signal will oscillate more than a million times during the interval T_2[27].

2.4 Bloch equations

In the development of NMR, Bloch proposed a set of differential equations to model the dynamics of the magnetization produced by nuclear magnetic dipoles in a magnetic field. As explained in the introduction section, the basic principles of NMR are based on the fundamental property of the spin. Therefore, for deriving the Bloch equation, we assume the magnetic spin to be placed in a static magnetic field $\mathrm{B_o}$, in the z direction. The magnetic moments orient either along field direction or it's opposite causes the spins to precess at the Larmor frequency.Hence the motion of an ensemble of independent spin one-half nuclei in a magnetic field may be described in terms of the spin magnetization vector, M. By definition, the magnetization is proportional to the angular momentum L.

$$\mathbf{M} = \gamma \mathbf{L} \tag{2.3}$$

The torque acting on the magnetization in a magnetic field B is given as, [7],

$$\tau = \frac{d\mathbf{L}}{dt} = \mathbf{M} \times B \tag{2.4}$$

Combining the above two equation leads to the equation governing the dynamics of magnetization vector M in the static magnetic field is then described using

$$\frac{d\mathbf{M}}{dt} = \gamma \mathbf{M} \times \mathbf{B_o}\hat{k}. \tag{2.5}$$

This equation indicates that the rate of change of magnetization is perpendicular to both M and $\mathbf{B_o}$, which implies that the initial spin precession is about the direction of the main magnetic field.

In order to change the plane of precession, the magnetization is tipped towards the transverse x-y plane. The factors affecting relaxation of the magnetization vector are the relaxation time constants T_1 and T_2 [29, 30]. As explained in the previous section, the spin-lattice relaxation time (denoted by T_1) corresponds to the time required for the system to return to its equilibrium value after it has been exposed to a 90^o tipping pulse. Similarly, the spin-spin relaxation time (denoted by T_2) depicts the time required for the tipped magnetization in the x-y plane to decay down to zero. The differential equation for magnetization in the presence of a magnetic field with relaxation terms can be combined to form a vector differential equation [31]. Hence, the Bloch equation becomes:

$$\frac{d\mathbf{M}}{dt} = \gamma \mathbf{M} \times \mathbf{B}_{ext} + \frac{1}{T_1}(M_o - M_z)\hat{k} - \frac{1}{T_2}(M_x\hat{i} + M_y\hat{j}), \tag{2.6}$$

where $\mathbf{B}_{ext} = B_o\hat{k}$ and $\mathbf{M} = M_x\hat{i} + M_y\hat{j} + M_z\hat{k}$. Since the external field components are zero along x and y directions, the cross product term in Equation (2.6) will be $(M_yB_o\hat{i} - M_xB_o\hat{j})$ and consequently, the equation becomes

$$\frac{d}{dt}(M_x\hat{i} + M_y\hat{j} + M_z\hat{k}) = \gamma(M_yB_o\hat{i} - M_xB_o\hat{j}) + \frac{1}{T_1}(M_o - M_z)\hat{k} - \frac{1}{T_2}(M_x\hat{i} + M_y\hat{j}). \tag{2.7}$$

Now, by equating the coefficients of $\hat{i}, \hat{j}$ and $\hat{k}$ on both sides of Equation (2.7), we get the relaxation phenomena governed by the following equation:

$$\frac{dM_z}{dt} = \frac{M_o - M_z}{T_1}, \tag{2.8}$$

$$\frac{dM_x}{dt} = \omega_o M_y - \frac{M_x}{T_2}, \tag{2.9}$$

and,

$$\frac{dM_y}{dt} = -\omega_o M_x - \frac{M_y}{T_2}. \tag{2.10}$$

The preceding equations describe relaxation and free precession when the only magnetic field acting on the magnetization is B_o. To describe what happens during the RF pulse, we must also include the effects of an oscillating field B_1. However in the NMR the signal is formed by applying the two fields that is the static field and RF field. When we add the influence of RF field the transmitter adds an oscillating magnetic field (B_1) along x- axis at a frequency ω.Then

$$\vec{B} = B_x\hat{i} + B_y\hat{j} + B_z\hat{k} = \left(B_1 \cos\omega t\hat{i} - B_1 \sin\omega t\hat{j} + B_0\hat{k}\right) \tag{2.11}$$

The expression of first order differential equation of Bloch equation in the laboratory frame in terms of individual component magnetization with relaxation terms can be written as follows [32].

$$\frac{dM_x}{dt} = \omega_0 M_y + \gamma B_1 \sin\omega t\ M_z - \frac{M_x}{T_2} \tag{2.12}$$

$$\frac{dM_y}{dt} = -\omega_0 M_x + \gamma B_1 \cos\omega t\ M_z - \frac{M_y}{T_2} \tag{2.13}$$

$$\frac{dM_z}{dt} = -\gamma B_1 \sin\omega t\ M_x - \gamma B_1 \cos\omega t\ M_y - \frac{(M_z - M_o)}{T_1} \tag{2.14}$$

This form of the equations clearly shows how the dynamics of the magnetization depends on four distinct rate constants: the angular frequency ω ; B_1 is the strength of RF pulse(we assume the amplitude of the pulse $b_1(\gamma\vec{B}_1) >> 0$); and the two relaxation rates, $\frac{1}{T_2}$, and $\frac{1}{T_1}$. M_o is equilibrium z magnetization for our case it can be ignored from the matrix.

Different proportions of these parameters produce a wide range of dynamics. For example, for biological tissues, T_1 may vary from 100 millisecond to 1 second (e.g. 900 ms for muscle and 250 ms for fat at 1.5 Tesla) whereas the T_2 may vary from 50 to 100 millisecond (e.g. 50 ms for muscle and 60 ms for fat at 1 Tesla).

In NMR experiment the widely used probes time scales from the nanosecond for spin precession to microsecond for molecular reorientation to milliseconds for spin-spin relaxation and up to the second spin-lattice relaxation and beyond that diffusion [33].

The inhomogeneous form of equation makes complicated for obtaining the analytical and numerical solutions to NMR and related problems. According to P.Allard et.al [34],they present two possible ways of avoiding the complication. The first and more familiar technique is to ignore relaxation during the application of RF pulses and to take account of relaxation only during periods of free precession. The second way is to avoid the overall relaxation effect.

The homogeneous form of the Bloch equation can be written as:

$$\frac{d}{dt}\begin{pmatrix} M_x \\ M_y \\ M_z \end{pmatrix} = \begin{pmatrix} -R_2 & \omega_0 & b_1 \sin \omega t \\ -\omega_0 & -R_2 & b_1 \cos \omega t \\ -b_1 \sin \omega t & -b_1 \cos \omega t & -R_1 \end{pmatrix} \begin{pmatrix} M_x \\ M_y \\ M_z \end{pmatrix} \tag{2.15}$$

Generally, in matrix form, the Bloch equation reads:

$$\frac{d}{dt}\mathbf{M}(t) = -A(t)\mathbf{M}(t), \tag{2.16}$$

where

$$\mathbf{A} = \begin{bmatrix} R_2 & -\omega_0 & -b_1 \sin \omega t \\ \omega_0 & R_2 & -b_1 \cos \omega t \\ b_1 \sin \omega t & b_1 \cos \omega t & R_1 \end{bmatrix} \quad \text{and} \quad \mathbf{M(t=0)} = \begin{bmatrix} 0 \\ 0 \\ M_o \end{bmatrix}. \tag{2.17}$$

Where M(t=0) is the intial magnetization before the application of pulse. Lastly, Equation $(2.12 - 2.14)$ form a system of first-order differential equations, so if the matrix A is constant in a time interval, they have an analytical solution in terms of the matrix exponential and initial states:

$$\mathbf{M}(t) = \mathbf{M}(0)e^{-\mathbf{A}t}. \tag{2.18}$$

For simple cases it is straightforward to compute a symbolic solution, but the full case offers some challenges. The approximate solutions of the Bloch equations will be the subject of Chapter 3.

CHAPTER 3
Methodology

3.1 Introduction

As explained elsewhere, the full solution of the Bloch equations is difficult to obtain and apply to simulations of NMR experiments. However, under special cases, solutions to these equations are well-known, but the full and exact solution is not trivial. In pulsed NMR, if we have free evolution (the RF term is zero), then the M_x and M_y oscillate at the Larmor frequency and relax at a rate of $\frac{1}{T_2}$ and the M_z relaxes back to its non-zero equilibrium value with a rate of $\frac{1}{T_1}$. If we have a long T_1, the change in the M_z is small. We can often treat the spin-lattice relaxation such that the M_z relaxes to zero, rather than a non-zero value, further simplifying the calculations. Under some conditions, we are solving a set of 3×3 matrix equations and provide an approximate solution by the eigen decomposition method.

3.2 Eigen decomposition method

As one can see from Equation (2.16), computing the exponential of a matrix A is a key computation for NMR. So, here in this section, we discusses on how to compute A by the eigen decomposition method. For simple cases, it is straightforward to compute a symbolic solution. A standard and general way of calculating a matrix exponential is to first obtain the eigenvalues and eigenvectors of the matrix,

$$D = U^{-1}AU, \tag{3.1}$$

where D is a diagonal matrix which represents the eigenvalues and the jth column of U is the vector of eigenvectors corresponding to the jth diagonal element of D. Then, we have

$$A = UDU^{-1}. \tag{3.2}$$

The matrix of eigenvectors of the original matrix also diagonalizes the exponential of the matrix[35],

$$e^{At} = Ue^{Dt}U^{-1}, \tag{3.3}$$

provided the original matrix is Hermitian, this is simple because the inverse of the matrix U is the conjugate transpose of the matrix U. Since the coefficient matrix A of the full homogeneous form is not Hermitian, both the eigenvalues and eigenvectors of A may be complex numbers. That is the imaginary part of the exponential gives the oscillation, while the real part gives the decay.

In general a linear transformation carries a vector $X = (x_1, x_2, \ldots, x_n)$ into a vector $Y = (y_1, y_2, \ldots, y_n)$. However, there may exist certain non-zero vectors for which AX is just X multiplied by a constant λ [36]:

$$AX = \lambda X. \tag{3.4}$$

That is, the transformation represented by the matrix (operator) A just multiplies the vector X by a number λ. Such a vector is called an eigenvector of the matrix A, and λ is called an eigenvalue or characteristic value of the matrix A. The problem of finding the eigenvalues and eigenvectors of a matrix is called an eigenvalue problem. Although there are various methods for the approximate determination of eigenvalues, here we only discuss the fundamental ideas and concepts that are important for the present study.

3.2.1 Determination of eigenvalues and eigenvectors

There are two parts to every eigenvalue problem. First, we compute the eigenvalue λ, given the matrix A. Next, we compute an eigenvector X for each previously computed eigenvalue λ. In this section, we will show that any square matrix of order n has at least 1 and at most n distinct (real or complex) eigenvalues. To this purpose, let us rewrite the system of Equation (3.4) as follows:

$$(A - \lambda I)X = 0, \tag{3.5}$$

where I is an identity matrix. This matrix equation consists of n homogeneous linear equations in the n unknown elements x_i of X:

$$\begin{array}{rrl} (a_{11} - \lambda)x_1 & a_{12}x_2 + \ldots & +a_{1n}x_n = 0 \\ a_{21}x_1 & (a_{22} - \lambda)x_2 + \ldots & +a_{2n}x_n = 0 \\ \vdots & \vdots & \vdots \\ a_{n1}x_1 + & a_{n2}x_2 + \ldots & +(a_{nn} - \lambda)x_n = 0 \end{array} \tag{3.6}$$

In order to have a non-zero solution, we recall that the determinant of the coefficients must be zero; that is,

$$\det(A-\lambda I)=\begin{bmatrix}(a_{11}-\lambda) & a_{12} & \dots & a_{1n}\\ a_{21} & (a_{22}-\lambda) & \dots & a_{2n}\\ \vdots & \vdots & \vdots & \vdots\\ a_{n1} & a_{n2}\dots & & (a_{nn}-\lambda)\end{bmatrix}=0. \tag{3.7}$$

The expansion of the determinant gives an n^{th} order polynomial equation in λ, and we write this as

$$c_o\lambda^n+c_1\lambda^{n-1}+c_2\lambda^{n-2}+\ldots+c_{n-1}\lambda+c_n=0, \tag{3.8}$$

where the coefficients c_i are functions of the elements a_{ij} of A. Equations (3.7) and (3.8) is called the characteristic equation.

Mathematically,once the eigenvalues have been found, corresponding eigenvectors can be found from the Equation (3.6). Since the system is homogeneous, if X is an eigenvector of A, then kX where k is any constant (not zero), is also an eigenvector of A corresponding to the same eigenvalue. Since $AX=\lambda X$, multiplying by an arbitrary constant k will give $kAX=k\lambda X$. Now, $kA=Ak$ (every matrix commutes with a scalar), so we have $A(kX)=\lambda(kX)$ showing that kX is also an eigenvector of A with the same eigenvalue λ. But kX is linearly dependent on X, and if we were to count all such eigenvectors separately, we would have an infinite number of them. Such eigenvectors are therefore not counted separately.
A formula for finding the inverse of a matrix U is given by

$$U^{-1}=\frac{adjU}{|U|}$$

Where adj$U$ is the adjoint matrix and $|U|$ is the determinant of of U. In order to find the adjoint of a matrix U

- first find the transpose of U by interchanging the rows and the columns of U.
- Next the minor of any element is obtained by covering up the elements in its row and column and obtaining the determinant of the remaining matrix. By substituting each element of U^T by its minor,we can write down a matrix of minors of U^T.
- the last step is finding the co-factor,taking its minor and imposing a place sign.In this three steps we can obtain the adjoint of matrix U.

3.3 Symbolic solution of the Bloch equations

In this subsection, we will concentrate on computing the exact symbolic solution of Equation (3.10). The exact eigenvalues of A are the roots of the characteristic polynomial associated with the matrix A, which is

$$P_A(\lambda) = det(A - \lambda I)$$

. After some mathematical manipulations, we get

$$P_A(\lambda) = \lambda^3 + (R_1 + 2R_2)\lambda^2 + (\omega^2 + b_1^2 + (2R_1 + R_2)R_2)\lambda + (b_1^2 R_2 + \omega^2 R_1 + R_1 R_2^2). \quad (3.9)$$

where I is an identity matrix. Here, in order to simplify expressions, we have substituted $R_1 = 1/T_1$, $R_2 = 1/T_2$ and $b_1 = \gamma B_1$ in the Bloch equations, respectively.

The eigenvalues of the matrix A are obtained by solving the equation $P_A(\lambda) = det(A - \lambda I) = 0$. This implies the eigenvalues are the roots of the cubic polynomial given by [37]

$$\lambda^3 + (R_1 + 2R_2)\lambda^2 + (2R_1R_2 + R_2^2 + \omega^2 + b_1^2)\lambda + (R_2{b_1}^2 + R_1\omega^2 + R_1R_2^2) = 0. \quad (3.10)$$

Although the solution to Equation (3.10) is not trivial, it is readily available elsewhere [38, 39]. That is,

$$\lambda = \begin{bmatrix} \lambda_1 \\ \lambda_2 \\ \lambda_3 \end{bmatrix}, \quad (3.11)$$

and,

$$\lambda_1 = \frac{\frac{1}{3}m + (1 + i\sqrt{3})n}{3 \times 2^{\frac{2}{3}}(o+p)^{\frac{1}{3}}(1 - \frac{1}{6\times 2^{\frac{1}{3}}}(1 - i\sqrt{3}))^{\frac{1}{3}}}, \quad (3.12)$$

$$\lambda_2 = \frac{\frac{1}{3}m + (1 - i\sqrt{3})n}{3 \times 2^{\frac{2}{3}}(o+p)^{\frac{1}{3}}(1 - \frac{1}{6\times 2^{\frac{1}{3}}}(1 + i\sqrt{3}))^{\frac{1}{3}}}, \quad (3.13)$$

$$\lambda_3 = \frac{\frac{1}{3}m - 2^{\frac{1}{3}}n}{3(o+p)^{\frac{1}{3}}(1 + \frac{1}{3\times 2^{\frac{1}{3}}})^{\frac{1}{3}}}, \quad (3.14)$$

in which

$$m = (-R_1 - R_2); \quad (3.15)$$

$$n = (3b_1^2 - R_1^2 + 2R_1R_2 - R_2^2 + 3\omega_0^2); \quad (3.16)$$

$$o = (9b_1^2R_1 - 2R_1^3 - 9b_1^2R_2 + 6R_1^2R_2 - 6R_1R_2^2 + 2R_2^2 - 18R_1\omega_0^2 + 18R_2\omega_0^2); \quad (3.17)$$

$$p = (\sqrt{4(n^3 + (o^2))}). \quad (3.18)$$

are real numbers. Similarly, $i = \sqrt{-1}$, $R_1 = 1/T_1$, $R_2 = 1/T_2$ and $b_1 = \gamma B_1$. We also see that the eigenvalue λ_3 is a real number and $\lambda_{1,2}$ are complex conjugates.

Since the computation of eigenvectors that corresponds to the matrix $\mathbb{A}$ are tedious, there are some shortcuts that we can use like Matlab inbuilt **eig** function. So, let us assume that v is the matrix of eigenvectors for A. Then, combining Equations (3.2) and (2.18) and substituting the eigenvalues and eigenvectors, we obtain:

$$M(t) = v\mathbf{diag}(e^{-\lambda_1 t}, e^{-\lambda_2 t}, e^{-\lambda_3 t})v^{-1}M(0), \tag{3.19}$$

where diagonal is dinoted by diag and λ_1, λ_2 and λ_3 are eigenvalues . Equation (3.19) is the general solution to the Equation (2.18). Note that the computations of both eigenvalues and eigenvectors will be carried out using Matlab 2017a inbuilt function for this study.

3.4 Approximate solutions of the Bloch equations

Approximate solution of the Bloch equations are obtained by assuming different cases as mentioned below.

3.4.1 Case 1:Free evolution ($b_1 = 0$)

In this case we apply the hard RF pulse for a very short period of time. The eigenvalues of the matrix A have simple expressions,

$$\lambda(A(b_1 = 0)) = \begin{bmatrix} \lambda_1 \\ \lambda_2 \\ \lambda_3 \end{bmatrix} = \begin{bmatrix} R_1 \\ R_2 - i\omega_o \\ R_2 + i\omega_o \end{bmatrix}, \tag{3.20}$$

where $\lambda(A(b_1 = 0))$ stands for the eigenvalues of the matrix A of b_1. In the Bloch equations,we ignore $b_1 = \gamma B_1 = 0$ then the homogeneous form of the Bloch equation can be written as:

$$\frac{d}{dt}\begin{pmatrix} M_x \\ M_y \\ M_z \end{pmatrix} = \begin{pmatrix} -R_2 & \omega_0 & 0 \\ -\omega_0 & -R_2 & 0 \\ 0 & 0 & -R_1 \end{pmatrix}\begin{pmatrix} M_x \\ M_y \\ M_z \end{pmatrix} \tag{3.21}$$

Each component of magnetization can be written as:

$$\frac{dM_x}{dt} = \omega_0 M_y - R_2 M_x \tag{3.22}$$

$$\frac{dM_y}{dt} = -\omega_0 M_x - R_2 M_y \tag{3.23}$$

$$\frac{dM_z}{dt} = -R_1 M_z \tag{3.24}$$

The equation of motion for M after the application of 90^0 pulse becomes:

$$M_x(t) = (M_x(0)cos(\omega_0 t) + M_y(0)sin(\omega_0 t))e^{-t/T_2} \tag{3.25}$$

$$M_y(t) = (M_y(0)cos(\omega_0 t) - M_x(0)sin(\omega_0 t))e^{-t/T_2} \tag{3.26}$$

$$M_z(t) = M_0(1 - e^{-t/T1}) \tag{3.27}$$

3.4.2 Case 2: Neglecting Relaxation

When we set $R_1 = 0 = R_2$ in the matrix A which represents the free precession, the eigenvalues of the matrix A become:

$$\lambda(A(R_1 = 0 = R_2)) = \begin{bmatrix} \lambda_1 \\ \lambda_2 \\ \lambda_3 \end{bmatrix} = \begin{bmatrix} 0 \\ -i\sqrt{b_1^2 + \omega^2} \\ i\sqrt{b_1^2 + \omega^2} \end{bmatrix}, \tag{3.28}$$

3.5 Fourier transformation

So far, we have seen how the precessing magnetization can be detected to give a signal which oscillates at the Larmor frequency - the free induction signal. We also commented that this signal will eventually decay away due to the action of relaxation; the signal is therefore often called the free induction decay (FID). But, the question is how do we turn this signal, which depends on time, into the a spectrum, in which the horizontal axis is frequency? This conversion is possible using a mathematical process known as Fourier transformation. The process takes the time domain function (the FID) and converts it into a frequency domain function (most commonly known as the spectrum) as shown in Fig.3.1. Like the time domain signal, the frequency domain signal has a real and an imaginary parts.

The real part of the spectrum shows what we call an absorption mode line, while the imaginary part of the spectrum gives a line shape known as the dispersion mode Lorentzian. This absorption line shape has a width at half of its maximum height of $\frac{1}{\pi T_2}$ Hz or $\frac{R_2}{\pi}$ Hz. This means that the faster the decay of the FID the broader the line becomes. However, the area under the line - that is the integral - remains constant so as it gets broader so the peak height reduces. The above points are clearly illustrated in Fig.3.1. This figure shows that the more rapidly the FID decays the broader the line in the corresponding spectrum.

Generally, the aim of Fourier transformation is to differentiate frequencies present in a complex waveform and to determine intensities corresponding to each frequency.

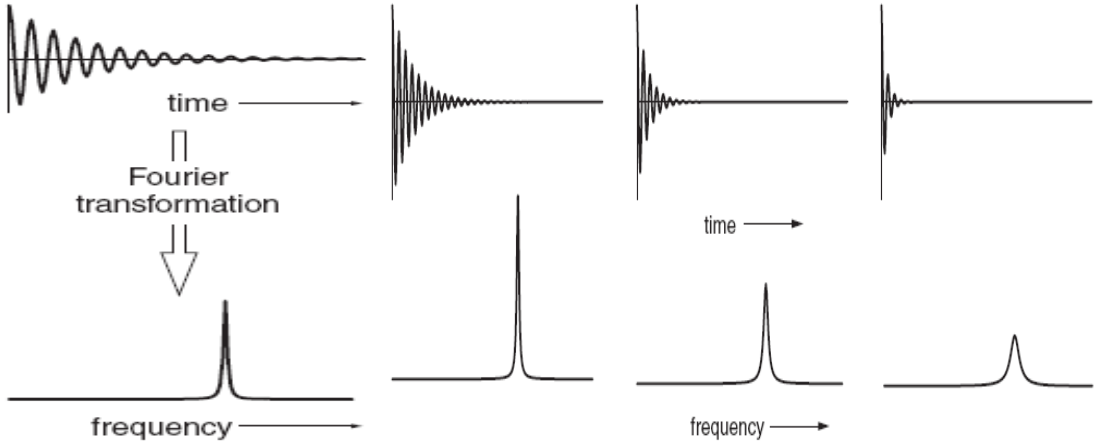

Figure 3.1: Fourier transformation is the mathematical process which takes us from the time domain to a function of frequency - the spectrum. A series of FIDs are shown at the top of the figure and below are the corresponding spectra, all plotted on the same vertical scale. The integral of the peaks remains constant, so as they get broader the peak height decreases.[40]

3.6 Matlab

In this study, the cost in computational time lies in the computation of the eigenvalues and eigenvectors of the matrix A. This computation can be achieved very quickly when using Matlab 2017a inbuilt function. The algorithm to compute an approximation of the solution to the Bloch equation for a given sample is highlighted as follows:

1. set duration of the pulse (t),
2. set the initial conditions $M_o\ \hat{z}$ for the Bloch equation,
3. set constants in the Bloch equation,
4. compute the eigenvalues, eigenvectors and inverse eigenvectors of the matrix A, and,
5. compute the evolution of the magnetisation vector M in the laboratory frame.

The Fourier transformation of the above computed signal is also carried out using Matlab 2017a inbuilt function. Generally, on the basis of this work, we have developed a matlab program that simulates the solution to the Bloch equations for protons in water and fat molecules in the laboratory frame. The Matlab program developed during this study can be obtained from the authors.

CHAPTER 4
Simulation Results and Discussion

As we have discussed so far different materials have different spin property so that their response to applied magnetic field is also different. Here, in this chapter, we present numerical results that illustrate the theoretical solutions for the time dependent Bloch equations discussed in the previous chapters.

4.1 Simulation of protons in water molecules

As explained elsewhere, some atomic nuclei are magnetic and each such nucleus is like a tiny weak bar magnet with North and South poles. The most magnetic nucleus is a single proton-the hydrogen nucleus (^1H), which is ubiquitous in tissue, mostly in the form of H_2O (water). Water is not normally magnetic, since the hydrogen protons are not lined up. The net magnetic field from protons pointing randomly in all directions is zero. The energy of random thermal motions of the water molecules keeps the protons pointing in random directions. Therefore, putting a water sample (or water-containing sample, such as a human subject) into a magnetic field will make the protons tend to line up with the magnetic field, just as the magnetic field from a large bar magnet can be used to align a small bar magnet. This tendency is weak compared to the randomizing effect of thermal motions, so the amount of alignment at any given moment is very small. However, applying a larger magnetic field will overcome the thermal agitation more and hence, resulting in more protons being aligned. The net effect is that the water becomes slightly magnetized itself, and the amount of magnetization is proportional to the strength of the applied field.

Figure 4.1 and 4.2 shows the time evolution of magnetization for protons in water molecules obtained by applying eigen decomposition method. These results are obtained by assuming that a sample of water is placed in a static magnetic field $B_o = 1.5$ T pointing along z-component. Here, in order to get a response from the object, the equilibrium magnetization is perturbed by applying a short RF field of 25 μT in the transverse plane with the excitation carrier frequency of the

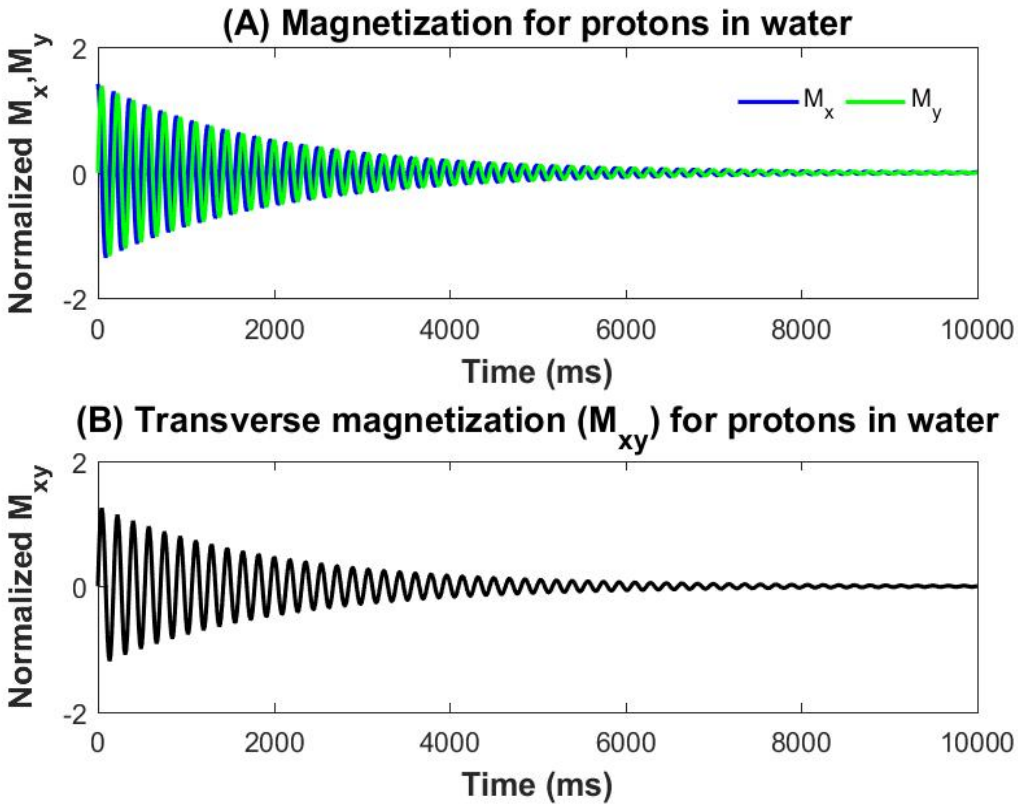

Figure 4.1: Time evolution of magnetization for protons in water molecules. For these plots, we used $T_1 = 4000$ ms, $T_2 = 2000$ ms, $\gamma = 267.54$ MHz/T, $B_o = 1.5$ T, $B_1 = 25$ μT, $\omega_o = \omega = 402$ MHz or f=64MHz.

RF pulse equal to the Larmor frequency of protons for water. As a result, M_o is flipped from its initial position towards the transverse plane and hence creating a transverse magnetization M_{xy} as shown in Fig. 4.1 (A). For instance, in MRI signal is proportional to the transverse magnetization.

The perturbation of M_o depends on the duration and magnitude of the RF field. For example, after the RF pulse is switched off, the magnetization precesses towards its equilibrium position. This process is known as relaxation, which is governed by T_1 and T_2. As stated in [41], we can accentuate these differences by changing how quickly we put in the radio frequency energy and how quick we choose to observe the signal coming back from the transverse magnetization of the precessing protons. This process indicates the free induction decay of water (see Figs. 4.1-4.6) and fat (see Figs. 4.7-4.9) and used to demonstrate these differences [42, 43]. It is also observed from Figs. 4.1 (A) and (B) that after time t longer than $T_2 = 2000$ ms, the signal is essentially gone. In other words, our results show that the solution

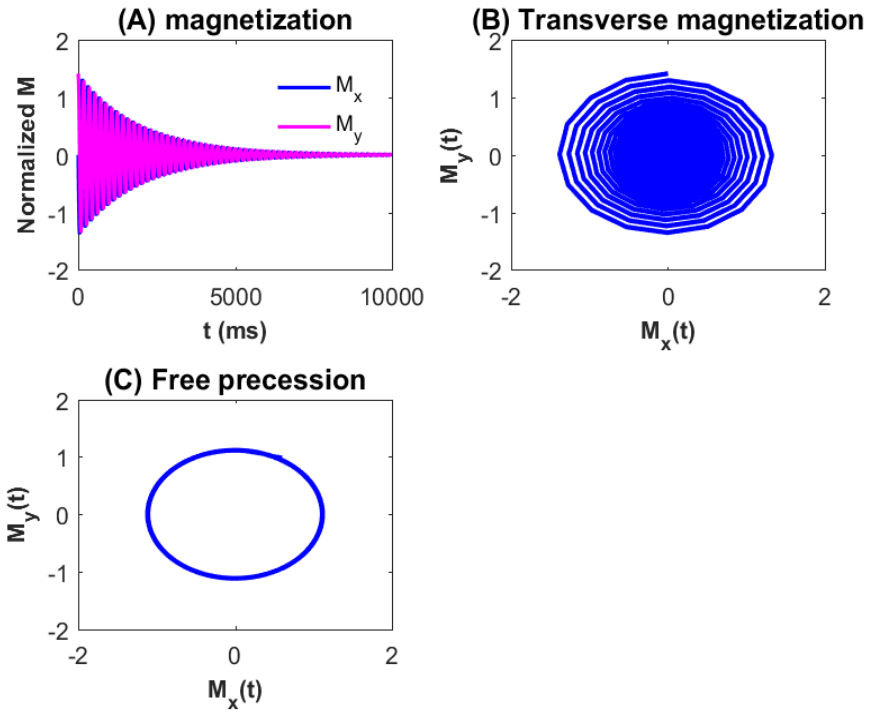

Figure 4.2: The dynamic relationship among different components of magnetization for protons in water molecules. For plots (A) and (B), we used the same inputs as 4.1. The plot in (C) is obtained by setting $1/T_1$ and $1/T_2 \to 0$ (neglecting relaxation), while other inputs are the same as with (A).

to $M_x(t)$ and $M_y(t)$ damped oscillatory and decays to zero (see Fig. 4.1 (A)). Since $M_x(t)$ and $M_y(t)$ are the x- and y-components of the transverse magnetization, the solution to $M_{xy}(t)$ (Fig. 4.1 (B)) also decays to zero. In general, the FID decays over time but in contrast the noise just goes on and on. Therefore, if we carry on recording data for long after the FID has decayed we will just measure noise and no signal.

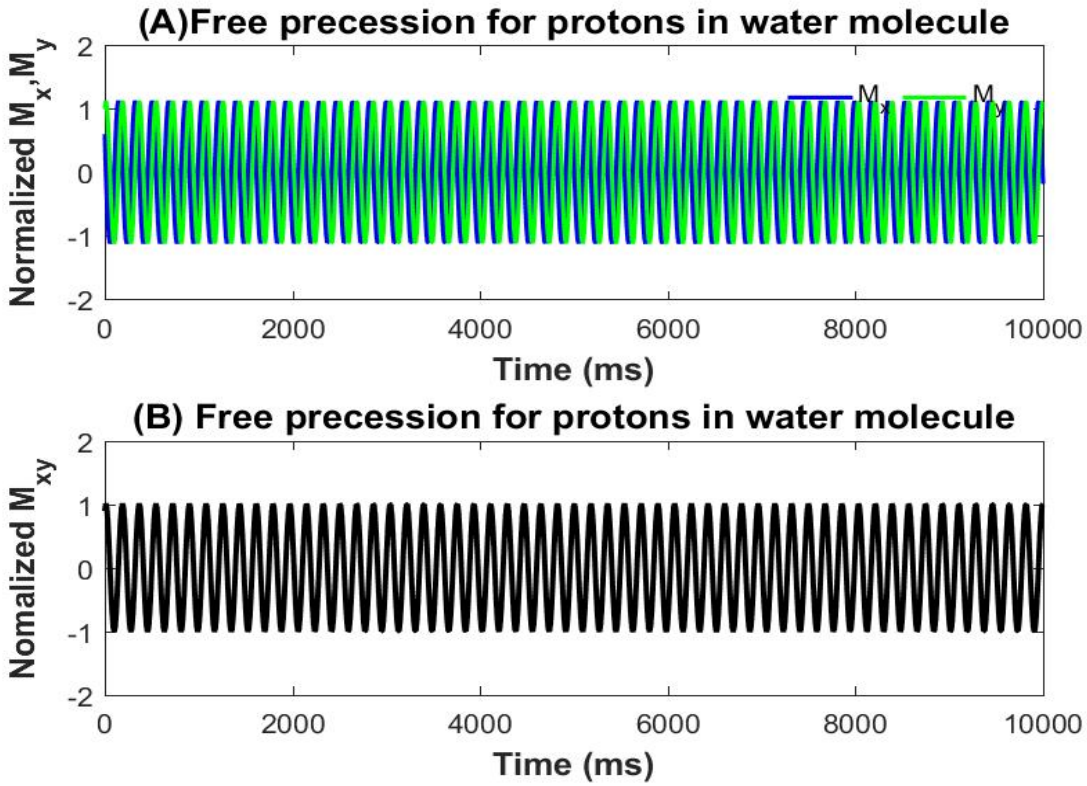

Figure 4.3: Simulation of the protons in water molecule obtained by setting $1/T_1$ and $1/T_2 \to 0$ (neglecting relaxation), while the other parameters are the same with 4.1.

Fig. 4.2 shows the dynamic relationship among different components of magnetization for protons in water molecules. Fig. 4.2 (A) shows the magnetization ($M(t)$ with respect to time. From this figure, it is observed that the transverse components of the relative magnetization decreases as time increases. In order to illustrate the dynamic relationship between the $M_x(t)$ and $M_y(t)$, these two components of magnetization are plotted in the complex plane and result shows a spiral structure , as shown in Fig. 4.2 (B). Fig. 4.2 (C) shows that the result of the free precession for protons in water molecules form a circular structure. Fig. 4.3 also shows that the protons in the water can hold onto their energy and continue to spin together in-phase, thus maintaining their transverse magnetization (see also Fig. 4.2 (C)). In other words their is interaction of spins with spins or the surrounding environment. In general, when neglecting relaxation terms (i.e., $1/T_1 = 1/T_2 = 0$), one obtains non-decaying oscillatory behaviour as shown in Fig. 4.3.

From previous chapter we see the case for spin system immdiately after RF pulse turned off. This figure indicates that the precession of magnetization around B at

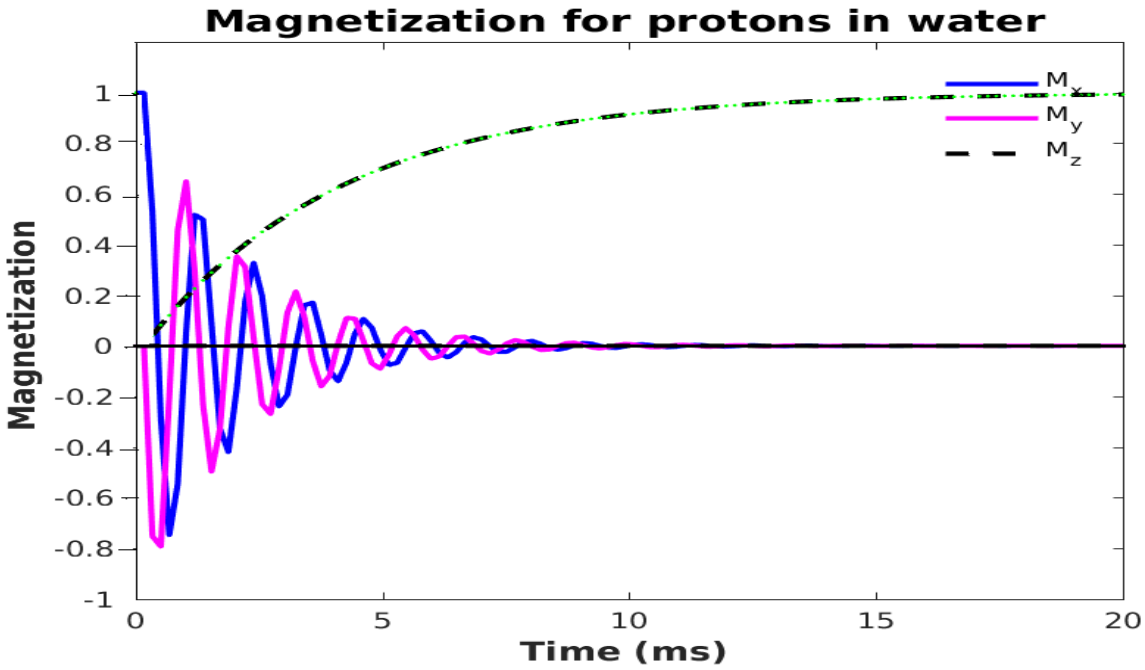

Figure 4.4: Plot of time evolution of magnetization for protons in water molecules immediately after hard RF pulse turned off . For these plots, we used $T_1 = 4000$ ms, $T_2 = 2000$ ms, $\gamma = 267.54$ MHz/T, $B_o = 1.5$ T, $M_x(0) = 0 = M_y(0)$ and $M_z(0) = 1$, $\omega_o = 402$ MHz or f=64MHz

the Larmor frequancy with decay of transverse magnetization (M_x, M_y) back to zero and regrowth of the longitudinal magnetization (M_z) to its original maximum value M_o. Because T_2 is always less than T_1, the transverse magnetization typically decay completely before the longitudinal magnetization is fully restored. T_1 represents the time required for M_z to grow from 0 to $(1 - 1/e)$, or about 63 % its final value. T_2 represents the time duration required for M_x or M_y to decay $1/e$ (or 37%) of their intial maximum values. In $Fig(4.5)$ the transverse component of magnetization (simply signal) immediately following the pulse are shown as a function of precessional frequency for 90^0 pulse.

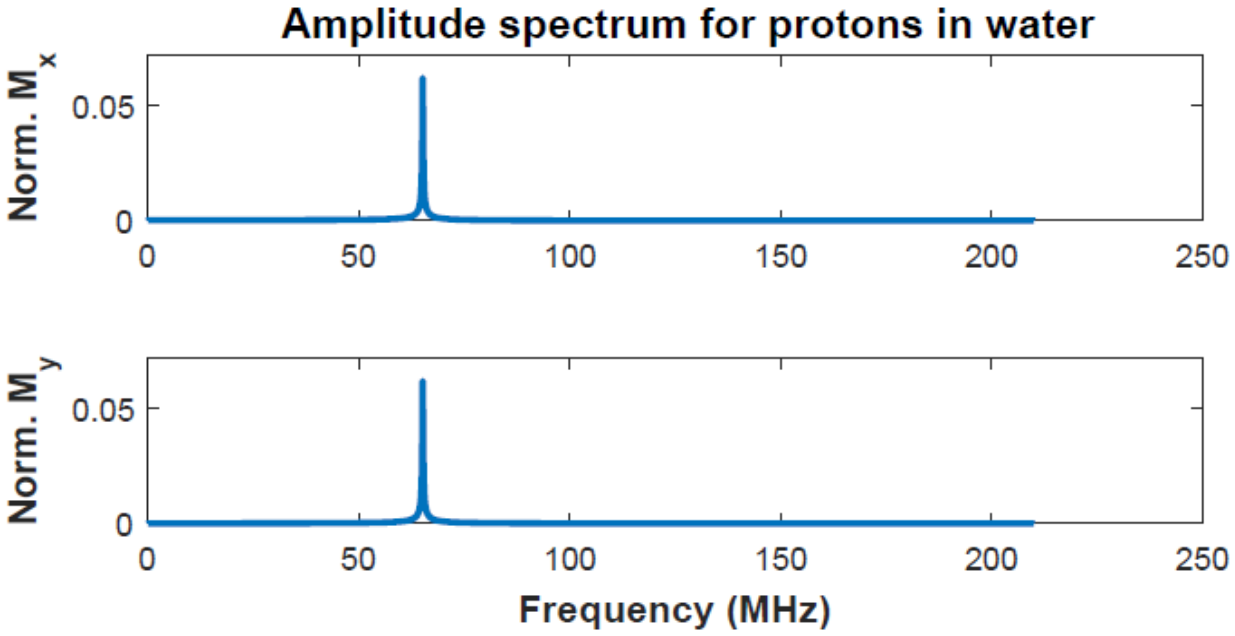

Figure 4.5: Normalized magnetization is denoted by Norm M_x,M_y.Plots of Fourier transformation of time domain signal for protons in water sample:frequency domain signal corresponding to the results displayed in Fig. 4.4

Fig. 4.6 shows the Fourier transformation of the time evolution of the magnetization components for protons in water molecules. In this figure, the frequency domain results $M_x(f)$, $M_y(f)$ and $M_{xy}(f)$ are shown from top to bottom, respectively.
The vertical axis in Fig. 4.6, shows the frequency domain signal that corresponds to the time domain signal given in Fig. 4.1. From Fig. 4.6 (A), we found that the intensity of water sample drops to zero for the frequencies approximately greater than 67.04 MHz and below 63 MHz and have maximum peak value in between these two values. In particular, we observed that the highest peak that the protons in water molecule precess with Precessional frequency of $\sim$64.29 MHz.

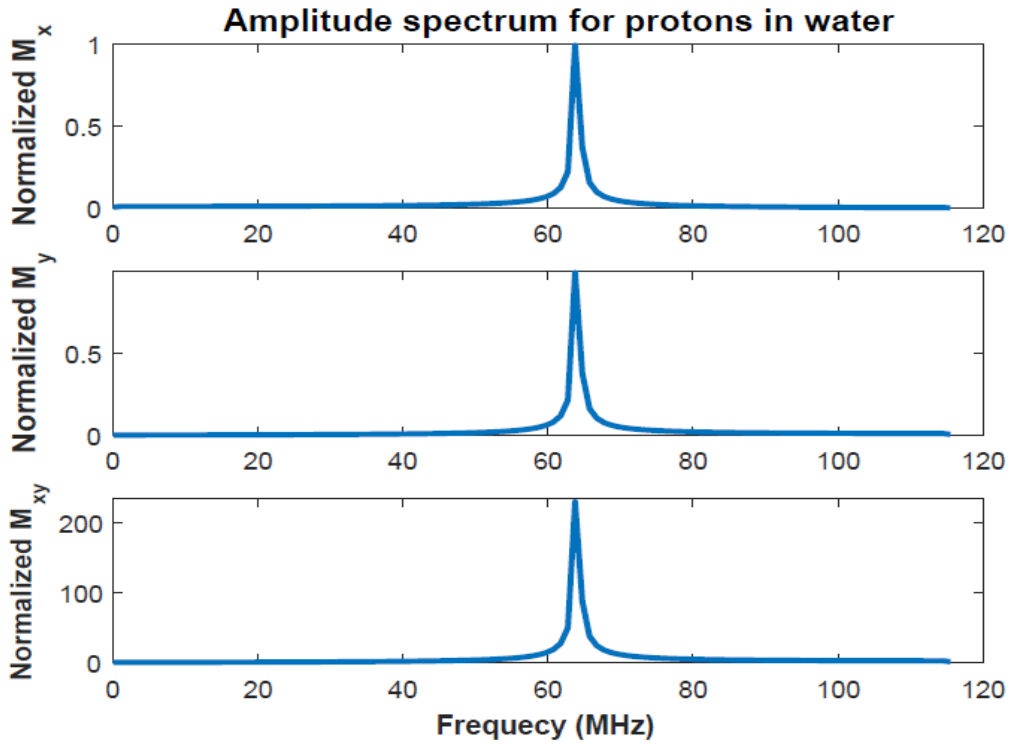

Figure 4.6: Fourier transformation of time domain signal for protons in water sample: frequency domain signal corresponding to the results displayed in Fig. 4.1

4.2 Simulation of protons in fat molecules

Signal from fat can play a critical role in determining the useful contrast of MR images in many situations. Here, the parameters used for the simulation of protons in fat molecules were chosen similar to water samples discussed in the previous section, except T_1 and T_2 are different from water samples. As in the case of water samples, the RF pulse is applied to disturb the protons so does in fat molecules so that they fall out of alignment with B_o. This disturbance occurs through the transfer of energy from the RF pulse to the protons in fat molecules. As mentioned in the previous section, this can only occur when the RF pulse has the same frequency as the Larmor (precessional) frequency [44, 45] of the protons in fat molecules.

The time evolution of magnetization components for protons in fat molecules obtained at $T_1 = 250$ ms and $T_2 = 60$ ms are shown in Fig. 4.7 (A and B).

When irradiated with a resonant radio frequency pulse, all protons in fat molecules absorb that energy, flip into the high energy state and spin together to produce transverse magnetization. Fat molecules (always known as triglycerides) are bulky

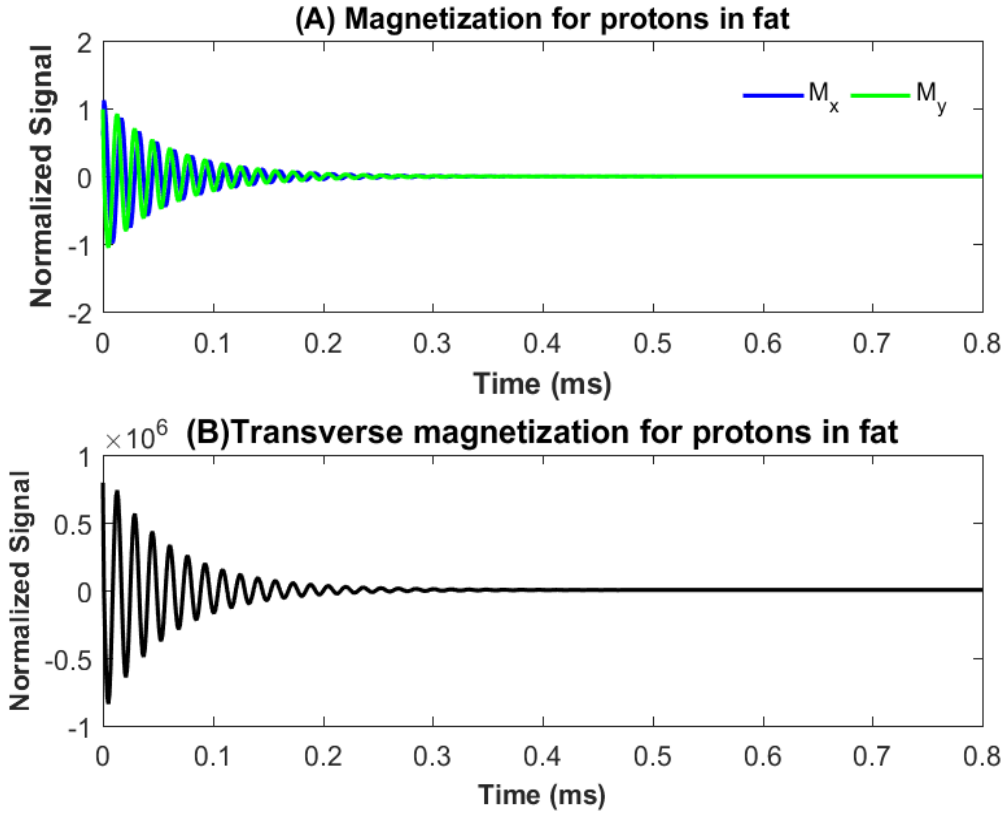

Figure 4.7: The same as Fig. 4.1, but for protons in fat molecules with $T_1 = 250$ ms and $T_2 = 60$ ms.

molecules with a molecular weight of 885.453 gm/mol that moves slowly, relax more rapidly as we observe in the above figure. The FID signal (the sum of $M_{xy}(t)$ during excitation) indicates the faster decay of the signal will be observed due to the interaction with neighbouring spin. Consequently due to shorter decay time signal the information that we are going to find about the molecule is not sufficient. After a sufficient amount of time, the protons will dephase by spin-spin relaxation process and the transverse magnetization vector will decay as shown in Fig. 4.7 (A and B). As we can see from Fig. 4.7 (A and B), a proton associated with the fat molecules being relatively bound molecules will decay rapidly as the spins push away from one another.

At first, the time evolution of the transverse components of the relative magnetization oscillates beyond unity, which could look non physical, as shown in Fig. 4.8 (A) (see also Fig. 4.2 (A)). But, the result never goes beyond unity as time inceases. The dynamic relationship between the $M_x(t)$ and $M_y(t)$ for protons in fat molecules are plotted in the complex plane (see Fig. 4.8 (B)) and our result shows that

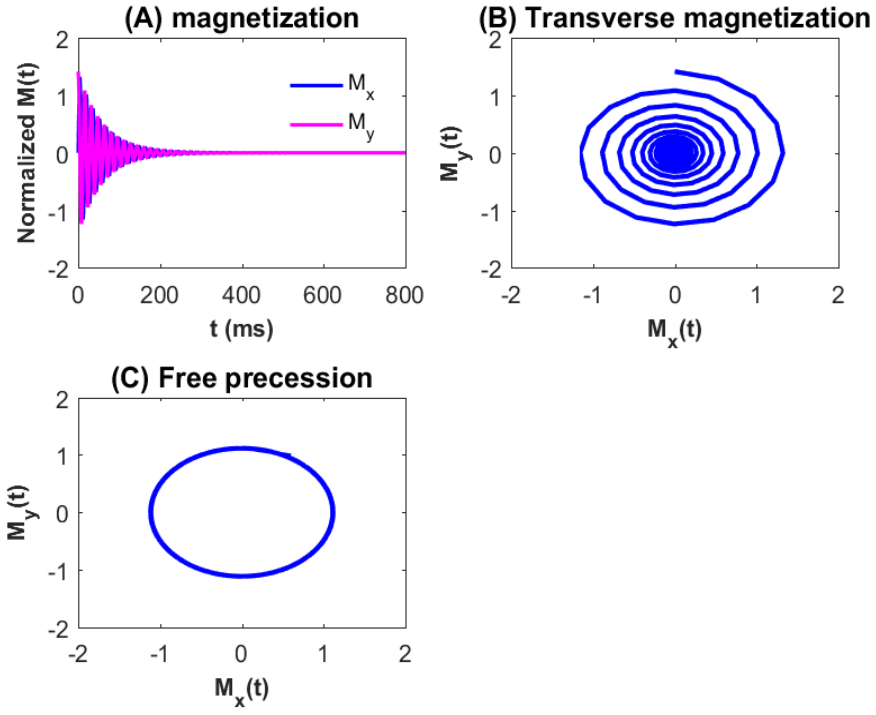

Figure 4.8: The dynamic relationship among different components of magnetization for protons in fat molecules. For plots (A) and (B), we used the same inputs as Fig.4.7. The plot in (C) is obtained by ignoring the relaxation terms, while other inputs are the same as with (A).

at time $t \sim T_2$ the spins get out of phase and the transverse magnetization will be destroyed.At a time $t >> T_1$ the effect of relaxation time will change these magnetization to reach its equilibrium value [40, 7]. Fig. 4.8 (C)) illustrates the simulation results that can be obtained when neglecting relaxations in fat samples. In general, both the decaying and non-decaying oscillatory parts of magnetization components shown in Figs. 4.7 and 4.8 have a structural behavior similar to the corresponding plots illustrated in Figs. 4.1 and 4.2.

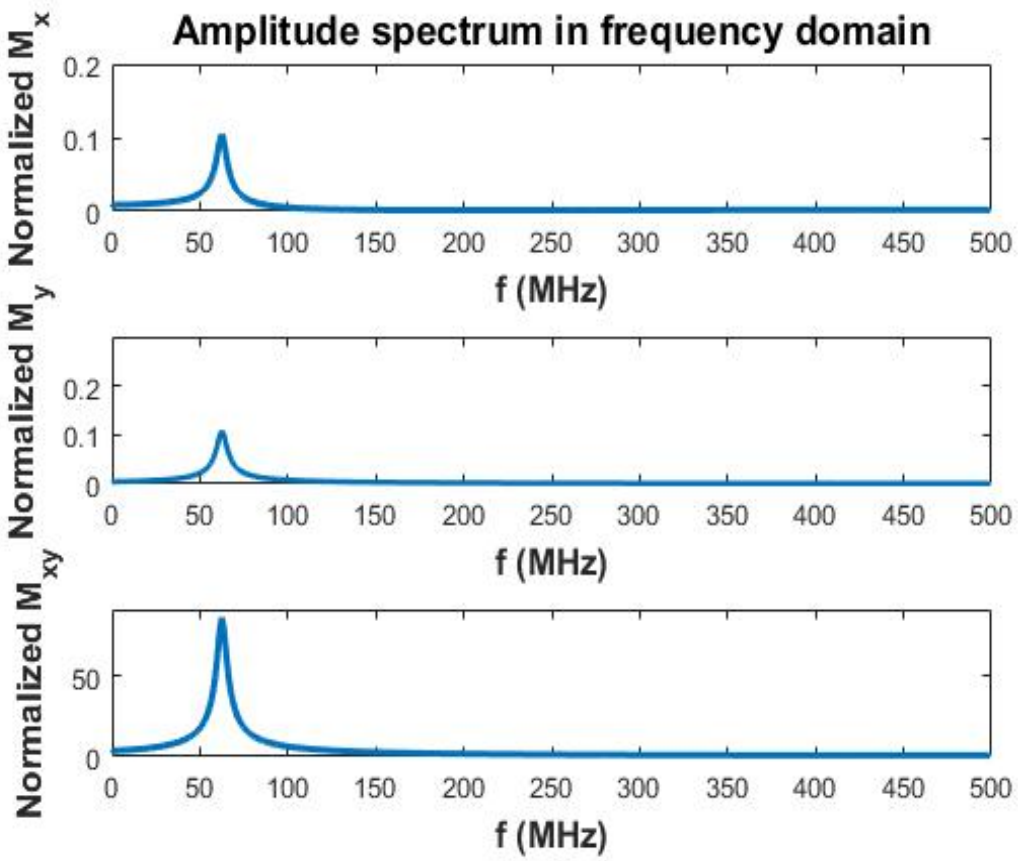

Figure 4.9: Plots of Fourier transformation signal for protons in fat sample. This transformation is done for the results displayed in Fig. 4.7.

Fig. 4.9 presents the frequency domain signal that corresponds to the time domain signal (the transverse component) displayed in Fig. 4.7. The RF pulse used to move the proton into a higher energy state is a frequency of 62.42 MHz. This indicates protons present in fat and water precess at a slightly different frequency due to their chemical environment. The electronic shielding of protons in fat (triglyceride) molecule is greater than water then the resulting proton resonance frequencies is broader than water as shown in the Fig. 4.9. Because we assume homogeneous magnetic field subjected to the entire sample they produce only one peak and this peak demonstrates the presence of detected hydrogen atom.

CHAPTER 5
Conclusion and Future work

5.1 Conclusion

The nucleus of the hydrogen atom (proton) has been most successfully exploited to produce high quality NMR images because of its desirable magnetic properties and the high concentration with which it is present in the body. Because these protons in our bodies have different local environments some associated with the free-flowing water molecules(smaller in molecular weight) while other are bound molecules associated with the structural or energy storing molecules of fat, they have characteristic differences in their T_1 and T_2 relaxations. In this study, we presented numerical solutions to the time-dependent Bloch equation for protons in water and fat molecules using eigen decomposition method (i.e., matrix operation). The computational cost of this method is simply the computation of the eigen-elements of a block tridiagonal matrix of very small size (3 x 3) using Matlab 2017a inbuilt function.

From different literatures, we found that the T_1 and T_2 values for protons in fat are much shorter than those of water molecules. This means that the processes that lead to recovery are much slower than those that lead to signal decay. A proton associated with the fat molecules being relatively fixed in position will decay rapidly as the spins push away from one another. On the other hand, protons in the water molecule can hold onto their energy and continue to spin together in phase, thus maintaining their transverse magnetization. At this point, we expect that the receiving coil is turned on and the signal coming back from the protons measured. The relatively large transverse magnetization in water, will give a strong signal, while smaller decay time then transverse magnetization in fat will give a weak signal. Implies that the information that we are going to find about the molecule is not sufficient. The protons present in fat and water precess at different frequency due to their chemical environment. The electronic shielding of protons in fat (triglyceride) molecule is greater than water then the resulting

proton resonance frequencies is broader than water. In contrast water molecule is less shielded molecule results in narrower and higher peak frequency signal. All the above mentioned are clearly observed from the numerical solutions presented in Chapter 3.
Therefore, based on the present study and other reviewed literatures, we concluded that a quantitative description of the MR signal produced by a particular tissue will depend on at least three intrinsic tissue parameters: the proton density, which determines M_o, and the relaxation times T_1 and T_2.

5.2 Future work

The work presented in this thesis suggests that there is much work to be performed to get the full numerical solutions to the Bloch equation. The following are some limitations of the present study:

- non-inclusion of the gradient field or time varying and multiple RF field;
- non-inclusion of main field inhomogeneity for realistic problem.

Therefore, in order to advance our understanding of NMR for complex systems, we plan to investigate the full numerical solutions to the generalized Bloch equations for protons in water and fat molecules by incorporating gradient, multiple RF pulse and main field inhomoginaty.

Bibliography

[1] Hayden, Michael, and Pierre-Jean Nacher. "History and physical principles of MRI." (2016).

[2] Weishaupt, Dominik, Victor D. Kochli, and Borut Marincek. How does MRI work?: an introduction to the physics and function of magnetic resonance imaging. Springer Science Business Media, 2008, 9-47.

[3] Blink, Evert J. "Basic MRI physics." 2nd. Retrieved 19.12 (2004): 2014.

[4] Bloch, Felix. The principle of nuclear induction. Kungl. boktryckeriet PA Norstedt soner, 1953.

[5] Carr, Herman Y., and Edward M. Purcell. "Effects of diffusion on free precession in nuclear magnetic resonance experiments." Physical review 94.3 (1954): 630.

[6] Van Vleck, J. H. "A third of a century of paramagnetic relaxation and resonance." Magnetic Resonance. Springer, Boston, MA, 1970. 1-10.

[7] Haacke, E. Mark, et al. Magnetic resonance imaging: physical principles and sequence design. Vol. 82. New York:: Wiley-Liss, 1999.

[8] Tansey, E. M., Daphne A. Christie, and Lois A. Reynolds. Wellcome Witnesses to Twentieth Century Medicine: Volume 2. Wellcome Trust, 1998.

[9] Mansfield, Peter, and Peter K. Grannell. "NMR'diffraction'in solids?." Journal of Physics C: solid state physics 6.22 (1973): L422.

[10] Nie, Zhenghua. Simulation and Optimal Design of Nuclear Magnetic Resonance Experiments. Diss. 2011.

[11] Bley, Thorsten A., et al. "Fat and water magnetic resonance imaging." Journal of Magnetic Resonance Imaging 31.1 (2010): 4-18.

[12] http://coolscienceexperimentshq.com

[13] Hancock, J. MRI Study Guide, Australian Institute of Radiography (2010).

[14] Das, T. P., and T. Ghose. "Magnetic properties of water molecule." The Journal of Chemical Physics 31.1 (1959): 42-52.

[15] Fischi Gomez, Elda. "Inhomogeneity Correction in High Field Magnetic Resonance Images: Human Brain Imaging at 7 Tesla." (2008).

[16] MRI: A Guided Tour. (2015, January 8). Retrieved from MAGLAB: https://nationalmaglab.org/education/magnet-academy/learn-the-basics/stories/mri-a-guided-tour.

[17] Zhenghui Zhang ,Field In-homogeneity Compensation In High Field Mangnetic RESONANCE IMAGING (MRI), thesis,1998

[18] Kasban, H., M. A. M. El-Bendary, and D. H. Salama. "A comparative study of imaging techniques." Int. J. Information Sci. Intelligent System 4 (2015): 37-58.

[19] Jhamb, Tanuj Kumar, Vinith Rejathalal, and V. K. Govindan. "A review on image reconstruction through mri k-space data." International Journal of Image, Graphics and Signal Processing 7.7 (2015): 42.

[20] Hinshaw, Waldo S., and Arnold H. Lent. "An introduction to NMR imaging: From the Bloch equation to the imaging e quation." Proceedings of the IEEE 71.3 (1983): 338-350.

[21] Funai, Amanda K. "Regularized Estimation of Main and RF Field Inhomogeneity and Longitudinal Relaxation Rate in Magnetic Resonance Imaging." (2011).

[22] Hidalgo-Tobon, S. S. "Theory of gradient coil design methods for magnetic resonance imaging." Concepts in Magnetic Resonance Part A 36.4 (2010): 223-242.

[23] Spectroscopy: Principles, Theory, Techniques and Applications, 7-17.

[24] Patton, James A. "MR imaging instrumentation and image artifacts." Radiographics 14.5 (1994): 1083-1096.

[25] Graf, Hansjorg, et al. "Effects on MRI due to altered rf polarization near conductive implants or instruments." Medical physics 33.1 (2006): 124-127.

[26] Grant PE., Vigneron DB., Barkovich, AJ. High resolution imaging of the brain. MRI Clin N Am 6: 139-154 (1998).

[27] Buxton, Richard B. Introduction to functional magnetic resonance imaging: principles and techniques. Cambridge university press, 2009.

[28] Rydell, Joakim. Advanced MRI data processing. Diss. Institutionen for medicinsk teknik, 2007.

[29] Jurczuk, Krzysztof, et al. "In silico modeling of magnetic resonance flow imaging in complex vascular networks." IEEE Trans. Med. Imaging 33.11 (2014): 2191-2209.

[30] Kwan, RK-S., Alan C. Evans, and G. Bruce Pike. "MRI simulation-based evaluation of image-processing and classification methods." IEEE transactions on medical imaging 18.11 (1999): 1085-1097.

[31] Bloch, Felix. "Nuclear induction." Physical review 70.7-8 (1946): 460.

[32] Bain, Alex D., Christopher Kumar Anand, and Zhenghua Nie. "Exact solution to the Bloch equations and application to the Hahn echo." Journal of Magnetic Resonance 206.2 (2010): 227-240.

[33] Bhalekar, Sachin, et al. "Fractional Bloch equation with delay." Computers Mathematics with Applications 61.5 (2011): 1355-1365.

[34] Allard, Peter, Magnus Helgstrand, and Torleif HÃd'rd. "The complete homogeneous master equation for a heteronuclear two-spin system in the basis of Cartesian product operators." Journal of Magnetic Resonance 134.1 (1998): 7-16.

[35] Murase, Kenya, and Nobuyoshi Tanki. "Numerical solutions to the time-dependent Bloch equations revisited." Magnetic resonance imaging 29.1 (2011): 126-131.

[36] Chow, Tai L. Mathematical Methods for Physicists: A concise introduction. Cambridge University Press, 2000.

[37] Nickalls, Richard WD. "A new approach to solving the cubic: Cardan's solution revealed." The Mathematical Gazette 77.480 (1993): 354-359.

[38] Morris, GARETH A., and PAUL B. Chilvers. "General analytical solutions of the Bloch equations. " Journal of Magnetic Resonance, Series A 107.2 (1994): 236-238.

[39] Madhu, P. K., and Anil Kumar. "Direct Cartesian-space solutions of generalized Bloch equations in the rotating frame." Journal of Magnetic Resonance, Series A 114.2 (1995): 201-211.

[40] Roberts, John D. "The Bloch equations. How to have fun calculating what happens in NMR experiments with a personal computer." Concepts in Magnetic Resonance 3.1 (1991): 27-45.

[41] Daphne Anne Pollacco, Magnetic Resonance Imaging, BSc Maths and Physics University of Malta, 2016

[42] Klioze, Doctor. "MRI: Basic Physics a Brief History." Retrieved from Youtube: https://www. youtube. com/watch (2013).

[43] Pooley, Robert A. "Fundamental physics of MR imaging." Radiographics 25.4 (2005): 1087-1099.

[44] Currie, Stuart, et al. "Understanding MRI: basic MR physics for physicians." Postgraduate medical journal 89.1050 (2013): 209-223.

[45] Assink, Roger Alan, Daniel Michael Mowery, and Mathias Christopher Celina. Sensitivity of proton NMR relaxation times in a HTPB based polyurethane elastomer to thermo-oxidative aging. No. SAND–2004-4382C. Sandia National Laboratories (United States). Funding organisation: US Department of Energy (United States), 2004.

DECLARATION

ADDIS ABABA UNIVERSITY
COLLEGE OF NATURAL AND COMPUTATIONAL SCIENCES
DEPARTMENT OF PHYSICS

MSc Thesis

Numerical Simulation of Bloch equation for protons in Water and Fat Molecules

Name of Candidate: Birtukan Asega Tadesse

I the under signed declare that the thesis is my original work and no part of it can be claimed as an intellectual property of anybody else except me and my advisors.

Signature: _____